

# Accepted Article

## 1 Resolving simulated sequences of earthquakes and fault 2 interactions: Implications for physics-based seismic 3 hazard assessment

4 Valère Lambert<sup>1</sup> and Nadia Lapusta<sup>1,2</sup>

5 <sup>1</sup>Seismological Laboratory, California Institute of Technology, Pasadena, California, USA

6 <sup>2</sup>Department of Mechanical and Civil Engineering, California Institute of Technology, Pasadena,  
7 California, USA

### 8 Key Points:

- 9 • Long-term interactions of fault segments qualitatively differ among fully versus  
10 quasi-dynamic simulations, and when using oversized cells.
- 11 • Simulations with similar stress drops and power-law frequency-magnitude statistics  
12 can have different rates of multi-segment ruptures.
- 13 • Simulated earthquake sequences can differ due to compounded effects of numerical  
14 errors, even when individual ruptures are well-resolved.

---

Corresponding author: Valère Lambert, [vlambert@caltech.edu](mailto:vlambert@caltech.edu)

This article has been accepted for publication and undergone full peer review but has not been through the copyediting, typesetting, pagination and proofreading process, which may lead to differences between this version and the Version of Record. Please cite this article as doi: [10.1029/2021JB022193](https://doi.org/10.1029/2021JB022193).

This article is protected by copyright. All rights reserved.

Accepted Article

15      **Abstract**

16      Physics-based numerical modeling of earthquake source processes strives to predict quantities  
17      of interest for seismic hazard, such as the probability of an earthquake rupture jumping  
18      between fault segments. How to assess the predictive power of numerical models remains  
19      a topic of ongoing debate. Here, we investigate how sensitive the outcomes of numeri-  
20      cal simulations of sequences of earthquakes and aseismic slip are to choices in numerical  
21      discretization and treatment of inertial effects, using a simplified 2-D crustal fault model  
22      with two co-planar segments separated by a creeping barrier. Our simulations demon-  
23      strate that simplifying inertial effects and using oversized cells significantly affects the  
24      resulting earthquake sequences, including the rate of two-segment ruptures. We find that  
25      fault models with different properties and modeling assumptions can produce similar  
26      frequency-magnitude statistics and static stress drops but have different rates of two-  
27      segment ruptures. For sufficiently long faults, we find that long-term sequences of events  
28      can substantially differ even among simulations that are well-resolved by standard consider-  
29      ations. In such simulations, some outcomes, such as static stress drops, are similar among  
30      adequately-resolved simulations, whereas others, such as the rate of two-segment ruptures,  
31      can be highly sensitive to numerical procedures and modeling assumptions. While it is  
32      possible that the response of models with additional ingredients ? realistic fault geometry,  
33      fluid effects, etc ? would be less sensitive to numerical procedures, our results emphasize  
34      the need to examine the potential dependence of simulation outcomes on the modeling pro-  
35      cedures and resolution, particularly when assessing their predictive value for seismic hazard  
36      assessment.

37      **Plain Language Summary**

38      There is growing interest in using computer simulations of long-term earthquake  
39      sequences to determine quantities of interest for seismic hazard, such as the probability  
40      of an earthquake rupture jumping from one fault segment to another. This is because  
41      large earthquakes are rare, hence the need to assess potential future earthquake scenarios  
42      through numerical modeling based on all available field observations and knowledge of fault  
43      physics. However, the outcomes of numerical simulations can depend on choices in model-

44 ing approximations and numerical procedures. Here, we numerically simulate earthquake  
45 sequences in a model with two fault segments separated by a barrier and study how the  
46 resulting earthquake sequences depend on common modeling choices. We find that different  
47 treatment of the inertial effects and small changes in physical and numerical parameters  
48 can result in different simulated long-term sequences, including significant changes in the  
49 rate of multi-segment ruptures. This is true even when certain properties of the earthquake  
50 sequences are similar, such as the earthquake frequency-magnitude statistics and the av-  
51 erage stress drop. Our results emphasize the need to examine how simulation outcomes  
52 may depend on modeling choices when assessing their predictive value and explore the  
53 sensitivity of hazard parameters to model uncertainty.

## 54 1 Introduction

55 Earthquakes occur in the context of fault networks and many large earthquakes  
56 span several fault segments. This reality brings about the issue of fault interaction and  
57 highlights the need for simulating earthquake source processes over several fault segments  
58 and regional-scale fault networks. How dynamic ruptures navigate fault segmentation has  
59 strong implications for seismic hazard analysis (Field, 2019; Biasi & Wesnousky, 2021).  
60 Earthquakes are capable of jumping fault segments. For example, the 1992 Landers earth-  
61 quake succeeded in rupturing across at least 4 fault segments, amounting to a Mw 7.3 event  
62 (Sieh et al., 1993). The 2016 Mw 7.8 Kaikoura earthquake ruptured at least 21 segments  
63 of the Marlborough fault system (Ulrich et al., 2019). Increasingly, seismological observa-  
64 tions show that it is not uncommon to see ruptures navigating and triggering subsequent  
65 ruptures within fault networks, including the recent 2019 Mw 6.4 and 7.1 Ridgecrest earth-  
66 quakes (Ross et al., 2019), and the 2012 Mw 8.6 and 8.2 Indian Ocean earthquakes (Wei  
67 et al., 2013), the largest and second-largest recorded strike-slip earthquakes to date. Yet,  
68 in any given seismogenic region, the record of past large events is not long enough to fore-  
69 cast the behavior of ruptures with respect to the existing fault segments, specifically how  
70 likely would the rupture be to jump between nearby segments, prompting the discussion on  
71 whether and how physics-based models may inform this and other questions important for  
72 seismic hazard assessment (Field, 2019).

Determining what conditions allow a dynamic rupture to propagate or arrest are key to understanding the maximum potential magnitude of an earthquake. Previous modeling of single fully dynamic ruptures have shown great success in investigating earthquake propagation in nonplanar and multi-segment fault models, including step-overs and branched geometries (Harris et al., 1991; Harris & Day, 1993, 1999; Kame et al., 2003; Duan & Oglesby, 2006; Dunham et al., 2011b; Galvez et al., 2014; Douilly et al., 2015; Lozos et al., 2015; Hu et al., 2016; Withers et al., 2018; Ando & Kaneko, 2018; Wollherr et al., 2019; Ulrich et al., 2019). In particular, such modeling has shown that the ability of a rupture to propagate across segments depends on the stresses before the rupture and shear resistance assumptions, as well as the geometry of the fault system. However, single-rupture simulations need to select initial conditions and need additional assumptions to incorporate the effect of previous seismic and aseismic slip.

Fault processes involve both sequences of dynamic events and complex patterns of quasi-static slip. Simulating this behavior in its entirety is a fascinating scientific problem. However, even for the more pragmatic goal of physics-based predictive modeling of destructive large dynamic events, it is still important to consider sequences of earthquakes and aseismic slip (SEAS), since prior slip events, including aseismic slip, may determine where earthquakes would nucleate as well as modify stress and other initial conditions before dynamic rupture. Furthermore, such simulations provide a framework for determining physical properties consistent with a range of observations including geodetically recorded surface motions, microseismicity, past (including paleoseismic) events, and thermal constraints, and hence may inform us about the current state of a fault segment or system and potential future rupture scenarios (e.g. Lapusta et al., 2000; Lapusta & Rice, 2003; Liu & Rice, 2005; Ben-Zion & Rice, 1997; Chen & Lapusta, 2009; Kaneko et al., 2010; Segall et al., 2010; Barbot et al., 2012; Noda & Lapusta, 2013; Erickson & Dunham, 2014; Erickson & Day, 2016; Jiang & Lapusta, 2016; Lambert & Barbot, 2016; Allison & Dunham, 2018; Lin & Lapusta, 2018; Cattania, 2019; Perry et al., 2020; Lambert et al., 2021). However, simulating long-term slip histories is quite challenging because of the variety of temporal and spatial scales involved.

Recently, several earthquake simulators have been developed with the goal of simulating millions of earthquake ruptures over regional fault networks for tens of thousands of

years (Tullis et al., 2012; Richards-Dinger & Dieterich, 2012; Shaw et al., 2018). The term "simulators" typically refers to approaches that employ significant simplifications, compared to most SEAS simulations, in solution procedures and physical processes, in order to simulate earthquake sequences on complex, regional scale 3-D fault networks for long periods of time. For example, earthquake simulators typically account only for the quasi-static stress transfer due to earthquake events, ignoring wave-mediated stress changes, aseismic slip/deformation, and fluid effects; employ approximate rule-based update schemes for earthquake progression instead of solutions of the governing continuum mechanics equations; and use oversized numerical cells. Such simplifications are currently necessary to permit simulations of hundreds of thousands of events over hundreds of fault segments that comprise the regional networks (Shaw et al., 2018). Earthquake simulators have matched a number of regional-scale statistical relations, including the Gutenberg-Richter frequency-magnitude scaling (Shaw et al., 2018), and highlighted the importance of large-scale fault and rupture interactions.

There is growing interest in using earthquake simulators to directly determine quantities of interest for seismic hazard, such as the probability of an earthquake rupture jumping from one fault segment to another (Shaw et al., 2018; Field, 2019). However, assessing the predictive power of numerical models remains a topic of active research. Determining how sensitive simulated outcomes may be to modeling choices and how reliably they can be determined from a given numerical model are topics of great importance for physics-based hazard assessment. Here, we examine the sensitivity of the long-term interaction of fault segments to choices in numerical discretization and representations of inertial effects in simulated sequences of earthquakes and aseismic slip, using a relatively simple 2-D model of two co-planar strike-slip fault segments separated by a velocity-strengthening (VS) barrier. We explore how considerations for adequate numerical resolution and convergence depend on the physical assumptions and complexity of earthquake sequences as well as on the modeling outcome of interest. We especially focus on the rate of earthquake ruptures jumping across the VS barrier and examine whether reproducing comparable earthquake frequency-magnitude statistics and static stress drops provides sufficient predictive power for the jump rate, a quantity of interest to seismic hazard studies (Field, 2019).

## 134 2 Model setup and numerical resolution

Our simulations are conducted following the methodological developments of Lapusta et al. (2000), Noda and Lapusta (2010) and Lambert et al. (2021). We consider a one-dimensional (1-D) fault embedded into a 2-D uniform, isotropic, elastic medium (Figure 1). The 2-D model approximates a faulted crustal plate coupled to a moving substrate using the idea of a constrained continuum (Lehner et al., 1981; Johnson, 1992). Fault slip may vary spatially along-strike but it is depth-averaged through a prescribed seismogenic thickness  $\lambda_S = 15$  km, beneath which the elastic domain is coupled to a substrate moving at the prescribed loading rate ( $V_{\text{pl}} = 10^{-9}$  m/s). The elastodynamic equation for the depth-averaged displacement along-strike  $\bar{u}(x, y, t)$  is given by (Lehner et al., 1981; Kaneko & Lapusta, 2008):

$$135 \quad Z^2 \frac{\partial^2 \bar{u}}{\partial x^2} + \frac{\partial^2 \bar{u}}{\partial y^2} + \frac{1}{\lambda_{\text{eff}}^2} \left( \frac{1}{2} \text{sign}(y) V_{\text{pl}} t - \bar{u} \right) = \frac{1}{c_s} \frac{\partial^2 \bar{u}}{\partial t^2}, \quad (1)$$

136 where  $\lambda_{\text{eff}} = (\pi/4)\lambda_S$  and  $Z = 1/(1-\nu)$ , with  $\nu$  being the Poisson's ratio. The effective wave speed along-strike for the crustal plane model is  $c_L = Z c_s$ , where  $c_s$  is the shear wave speed. 137 The along-strike slip is then given by  $\delta(x, t) = \bar{u}(x, y=0^+, t) - \bar{u}(x, y^-, t)$ .

138 Our simulations resolve sequences of earthquakes and aseismic slip (SEAS) in their 139 entirety, including the gradual development of frictional instability and spontaneous nucleation, dynamic rupture propagation, post-seismic slip that follows the event, and the 140 interseismic period between events (Figure 2). In all models, frictional resistance along the 141 fault interface is governed by the standard laboratory-derived rate-and-state friction law 142 with the state evolution described by the aging law (Dieterich, 1979; Ruina, 1983): 143

$$\tau = \bar{\sigma} f = (\sigma - p) \left[ f_* + a \ln \frac{V}{V_*} + b \ln \frac{V_* \theta}{D_{\text{RS}}} \right], \quad (2)$$

$$\frac{d\theta}{dt} = 1 - \frac{V \theta}{D_{\text{RS}}}, \quad (3)$$

144 where  $\bar{\sigma} = (\sigma - p)$  is the effective normal stress,  $\sigma$  is the normal stress,  $p$  is the pore pressure, 145  $\tau$  is the shear stress,  $f$  is the friction coefficient,  $V$  is the slip velocity,  $\theta$  is the state variable, 146  $D_{\text{RS}}$  is the characteristic slip for the evolution of the state variable,  $f_*$  is the reference 147 steady-state friction coefficient corresponding to a reference slip rate  $V_*$ , and  $a$  and  $b$  are 148 the direct and evolution effect constitutive parameters, respectively.

149 At steady-state (constant slip velocity), the shear stress and state variable evolve to  
 150 their steady-state values  $\tau_{ss}$  and  $\theta_{ss}$  given by:

$$\tau_{ss}(V) = (\sigma - p) \left[ f_* + (a - b) \ln \frac{V}{V_*} \right], \quad (4)$$

$$\theta_{ss}(V) = \frac{D_{RS}}{V}. \quad (5)$$

151 The combination of frictional properties such that  $(a - b) > 0$  results in steady-state velocity-  
 152 strengthening (VS) behavior, where the shear resistance increases with an increase in slip  
 153 velocity and where stable slip is expected. If  $(a - b) < 0$  then the fault exhibits velocity-  
 154 weakening (VW) behavior, in which case an increase in slip velocity leads to a decrease  
 155 in shear resistance, making these regions of the fault potentially seismogenic if their size  
 156 exceeds a critical nucleation size.

157 Two theoretical estimates of the nucleation size in mode II are (Rice & Ruina, 1983;  
 158 Rubin & Ampuero, 2005):

$$h_{RR}^* = \frac{\pi}{4} \frac{\mu L}{(1-\nu)(b-a)(\sigma-p)}; \quad h_{RA}^* = \frac{2}{\pi} \frac{\mu L b}{(1-\nu)(b-a)^2(\sigma-p)}, \quad (6)$$

159 where  $\mu$  is the shear modulus. The estimate  $h_{RR}^*$  was derived from the linear stability anal-  
 160 ysis of steady frictional sliding by Rice and Ruina (1983). It also represents the critical cell  
 161 size for steady-state quasi-static sliding such that larger cells can become unstable on their  
 162 own. Thus  $h_{RR}^*$  represents a key length scale to resolve for slow interseismic processes and  
 163 earthquake nucleation (Rice & Ruina, 1983; Lapusta et al., 2000). The estimate  $h_{RA}^*$  was  
 164 determined in the parameter regime  $a/b > 0.5$  using the energy balance of a quasi-statically  
 165 expanding crack (Rubin & Ampuero, 2005), and provides an estimate of the minimum size  
 166 for a slipping region that releases enough stored energy to result in the radiation of waves.

167 We aim to explore the impact of numerical resolution on the long-term simulated slip  
 168 behavior of sequences of earthquakes and aseismic slip. The nucleation size,  $h^*$ , estimated  
 169 by either  $h_{RR}^*$  or  $h_{RA}^*$  from equation (6), is one length-scale that clearly needs to be well  
 170 resolved. Early resolution studies for sequences of events showed that resolution of the  
 171 nucleation scale  $h_{RR}^*$  by 20 to 40 cells is required for stable numerical results (Lapusta et  
 172 al., 2000). Later, the need to resolve the nucleation size by at least 20 cells was shown to

be due to the more stringent criterion of resolving the region where shear resistance breaks down at the rupture front, often referred to as the cohesive zone. The cohesive zone can be an order of magnitude smaller than the nucleation size, depending on the constitutive description (Day et al., 2005; Lapusta & Liu, 2009). The size of the cohesive zone depends on the weakening rate  $W$  of shear stress with slip associated with the constitutive law. The quasi-static estimate  $\Lambda_0$  of the cohesive zone size at near-zero rupture speed and constant  $W$  is given by:

$$\Lambda_0 = C_1 \frac{\mu'}{W}, \quad (7)$$

where  $C_1$  is a constant,  $\mu' = \mu$  for mode III, and  $\mu' = \mu/(1 - \nu)$  for mode II (Rice, 1980). For standard rate-and-state friction with the aging form of the state variable evolution, the weakening rate is given by  $W = D_{\text{RS}}/(b\bar{\sigma})$  (Lapusta & Liu, 2009) and:

$$\Lambda_0 = C_1 \frac{\mu' D_{\text{RS}}}{b\bar{\sigma}}. \quad (8)$$

If one assumes that the traction distribution within the cohesive zone is linear, then the constant  $C_1$  can be approximated as  $C_1 = 9\pi/32$  (Rice, 1980).

For fully dynamic rupture simulations, continuously resolving the breakdown process at the rupture front becomes even more challenging as the cohesive zone size  $\Lambda$  exhibits a contraction with increasing rupture speed  $v_R$  (e.g Rice, 1980):

$$\Lambda = \Lambda_0 A^{-1}(v_R); \quad A_{II}^{-1} = \frac{(1-\nu)c_s^2 \mathcal{D}}{v_R^2(1-v_R^2/c_s^2)^{1/2}}; \quad A_{III}^{-1} = (1-v_R^2/c_s^2)^{1/2}, \quad (9)$$

where  $\mathcal{D} = 4(1-v_R^2/c_s^2)^{1/2}(1-v_R^2/c_p^2)^{1/2} - (2-v_R^2/c_s^2)^{1/2}$  with  $c_p = \sqrt{2(1-\nu)/(1-2\nu)}c_s$ . Note that  $A^{-1}(0^+) = 1$ , giving the quasi-static cohesive zone estimate  $\Lambda_0$  when  $v_R = 0^+$ . As the rupture speed approaches the limiting wave speed,  $v_R \rightarrow c_R$  (Rayleigh wave speed) for mode II and  $v_R \rightarrow c_s$  (shear wave speed) for mode III, one has  $A^{-1}(v_R) \rightarrow 0$  and the width of the breakdown region approaches zero. Hence it becomes increasingly more challenging to resolve the rupture front during fully dynamic simulations if the rupture accelerates towards the limiting speeds. Such acceleration typically occurs during long enough propagation of dynamic rupture over favorable prestress, unless impeded by additional factors such as unfavorable prestress or situations with increasing effective breakdown energy, e.g.,

due to off-fault inelasticity or navigating fault roughness (Poliakov et al., 2002; Andrews, 2005; Rice, 2006; Okubo et al., 2019; Dunham et al., 2011b; Perry et al., 2020; Lambert & Lapusta, 2020). Simulations of faults with rate-and-state friction and the aging form of the state variable evolution embedded in elastic bulk result in ruptures with near-constant breakdown energy (Perry et al., 2020) and this holds for most cases considered in this study. In section 7, we show that adding an approximation of off-fault inelasticity to our simulations that reduces the rupture speeds does not alter our conclusions.

In our model, the fault contains a frictional domain consisting of two VW regions of length  $\lambda_{VW} = 32$  km that are separated by a 2-km-long VS region that impedes rupture propagation. We select large enough values of the velocity strengthening in the central VS region so that the region acts like a barrier, requiring ruptures to jump/renucleate on the other side of the barrier to propagate over the second segment. This region is a proxy for what would be a gap in the fault connectivity, at least at the surface, requiring the ruptures to jump across. The remainder of the frictional region surrounding the VW segments has more mild VS properties (Figure 1). At the edges of the model, outside of the frictional domain, fault slip is prescribed at the loading plate rate. Values for the model parameters used in our simulations are provided in Tables 1 and 2. We first examine models with lower instability ratio  $\lambda_{VW}/h_{RR}^*$  that result in quasi-periodic sequences of events, and then consider models with higher instability ratios that result in more complex earthquake sequences and qualitatively different convergence behavior.

### 3 Resolving quasi-periodic fully dynamic sequences of earthquakes and aseismic slip (SEAS)

Let us consider the simulated slip behavior of fault model M1 with instability ratio  $\lambda_{VW}/h_{RR}^* = 21$  (Table 2). Its quasi-static cohesive zone ( $\Lambda_0 = 1.1$  km) should be well-resolved by cell sizes of 12.5 and 25 m, with 88 and 44 cells over  $\Lambda_0$ , respectively; the nucleation size is even larger and hence also well-resolved. Consistently with these considerations, these two well-discretized simulations produce the same relatively simple quasi-periodic sequences of earthquake events that periodically jump across the VS barrier

(Figure 2A & B). We clearly see that the results are the same for the two simulations with different resolutions, including the local evolution of slip rate and shear stress during ruptures late in the earthquake sequence (Figure 2D-E). Note that the cohesive zone evolves throughout the rupture process, shrinking with the increasing rupture speed by 3-4 times in these simulations (Figure 2F-H) and the spatial discretization is fine enough to adequately characterize the rupture front throughout the entire dynamic process. The jump rate for both simulations is 0.54; we define this rate of ruptures jumping across the VS barrier within a given time period as the total number of ruptures that propagate towards the barrier and result in seismic slip on both fault segments divided by the total number of ruptures that propagate towards the barrier and span at least the segment on which they nucleate.

The variability between different ruptures in fault model M1 is generally mild, as shown by their frequency-magnitude histograms (Figure 2C). To create the frequency-magnitude histograms, we compute the moment for each simulated event in our 2-D models as  $M = \mu\bar{\delta}A$  where the rupture area is defined with respect to the rupture length  $L_R$  and seismogenic depth  $\lambda_S$ , as  $A = (\pi/4)L_R^2$  when  $L_R \leq \lambda_S$  and  $A = L_R\lambda_S$  when  $L_R > \lambda_S$ .

The quasi-periodic nature of events observed over the first 4000 years in well-resolved simulations of fault model M1 persists in longer-duration simulations over 20,000 years, resulting in similar long-term jump rates of 0.48 to 0.54 depending on the time interval considered (Figure 3). We also examine simulations of fault model M1 with different initial shear stress conditions and find that the long-term sequences of events converge to the same quasi-periodic behavior upon adequate discretization, despite the initial few events being different (Figure 3A vs B; details of initial shear stress distributions S1 and S2 are provided in the Supplementary Materials). Simulations of fault model M1 thus exhibit *long-term numerical convergence* upon adequate discretization, producing virtually indistinguishable long-term slip behavior and a consistent rate of two-segment ruptures among simulations with differing initial conditions, after a sufficiently large initial sequence of events.

Let us now consider simulations that use larger computational cells. The cell sizes of 250 m and 125 m resolve the quasi-static cohesive zone  $\Lambda_0$  with 4.5-9 cells (Figure 4). While this resolution seems adequate, one can anticipate that the dynamic shrinking of

the cohesive zone size by 3-4 times would result in a more marginal resolution of 1-3 cells. Indeed, we see that the simulated long-term sequences of events and jump rates differ substantially from those of the well-resolved simulations (Figures 2A & B vs. 4A & B). Considering even larger cell sizes of 500 m and 1000 m brings further differences in the event sequences and jump rates (Figure 5), with the earthquake sequences that look plausible and not obviously numerically compromised even for the largest cell sizes (Supplementary Figure S1). Note that the jump rate in simulations with marginal and oversized cells is neither systematically larger nor smaller than the range 0.48-0.54 from the well-resolved cases, but varies from 0.25 to 0.95 depending on the choice of numerical discretization.

Increasingly poor resolution of the dynamic cohesive zone at the rupture front and, for the largest cell sizes, of the nucleation zone results in an increasing abundance of small events (Figure 5), as had been shown in previous studies (Rice, 1993; Rice & Ben-Zion, 1996; Lapusta & Liu, 2009). Inadequate resolution of the dynamic rupture front prevents simulating the actual stress concentration and promotes event arrest. Inadequate resolution of the nucleation size enables individual cells or small number of cells to fail independently due to the inadequate resolution of the stress interactions (Rice, 1993; Rice & Ben-Zion, 1996; Lapusta & Liu, 2009). Using sufficiently oversized cells can result in power-law statistics in terms of the frequency-magnitude distribution of simulated earthquake ruptures (Figure 5E-J; Rice, 1993; Rice & Ben-Zion, 1996).

Note that the suggested minimum average resolution of 3 cells of the (variable) cohesive zone from the dynamic rupture study by Day et al. (2005) is not adequate for convergent results in these earthquake sequence simulations. That criterion would be achieved in this model for a cell size between the 250 m and 125 m. Yet the simulated long-term behavior for those cell sizes is clearly different from the better-resolved and convergent results with the cell sizes of 25 m and 12.5 m. At the same time, the criterion by Day et al. (2005) works well for a single dynamic rupture as intended, since the first dynamic events in simulations with cell sizes 12.5 m, 25 m, 125 m, and 250 m are quite similar to each other (Supplementary Figure S2). The events are not identical, however; for example, the average slip with the resolution of 12.5 m and 125 m differs by 0.7%. Clearly, these differences - acceptable for a single event - accumulate in these highly nonlinear solutions, resulting in different event statistics and jump rate (Figure 5).

We find that our fully dynamic 2-D simulations of fault model M1, which include uniform VW properties with relatively mild weakening due to standard rate-and-state friction, converge when the quasi-static cohesive zone estimate  $\Lambda_0$  is discretized by at least 22 cells, which translates to the average resolution of the dynamically variable cohesive zone size of 10-15 cells. Fault models with additional or different ingredients, such as fault heterogeneity/roughness, more efficient weakening, 3D elastodynamics with 3D faults, or different instability ratio, would require further considerations for resolution requirements that result in convergent simulations. For example, as we discuss in section 6, the convergence and resolution properties of models with higher instability ratios, which result in more complex earthquake sequences, are qualitatively different.

In the more complicated earthquake sequences observed in under-resolved simulations of fault model M1, some statistics, such as the rate of two-segment ruptures, depends on the specific period that one considers throughout the simulation. To explore the variability in the event statistics and jump rate across the VS barrier in models with different numerical resolution, we examine the jump rate over different 2000-year periods throughout longer term simulations of 20,000 years, using a sliding window of 1000 years starting at the beginning of the simulation (19 periods total; Figure 5). The choice of a 2000-year period allows us to have a sufficient number ( $\sim 20$ ) of large earthquakes within a period to estimate jump rates. We also consider the outcomes for two different initial conditions S1 and S2, as before. For the well-resolved simulations exhibiting long-term convergence, the frequency-magnitude and 2000-year jump rate statistics for simulations with different initiation conditions are comparable, with the jump rate for all 2000-year periods being consistent with the overall 20,000 year jump rate (Figure 5A-B). As the numerical resolution worsens, the sequences of events become more complex with greater variability in rupture sizes and increased production of smaller events (Figure 5C-J). The jump rate during any 2000-year period also becomes more variable in marginally-resolved simulations and can considerably differ from both the 20,000-year jump rate of the same simulation as well as from the true jump rate in the well-resolved simulations. Note that, despite being clearly affected by numerical resolution, the frequency-magnitude and jump-rate distributions of inadequately resolved simulations can appear generally consistent among simulations with similar cell sizes and different initial conditions (Figure 5 left vs. right columns). In other

words, even if simulations using marginal or oversized cells produce comparable statistical properties for different initial conditions, these characteristics do not necessarily represent robust features of the physical system but rather may still be numerical artifacts.

## 4 Interaction of fault segments in simulations with quasi-dynamic approximation for inertial effects

Many numerical studies of long-term fault behavior utilize quasi-dynamic solutions to the equations of motion, in which the wave-mediated stress transfers during the co-seismic phase are replaced with a radiation damping approximation (Rice, 1993). The quasi-dynamic approximation substantially reduces the computational expense of the simulation, as the consideration of stress redistribution by waves requires substantial additional storage and computational expense. Considerable insight into fault mechanics has been derived from studies using quasi-dynamic formulations, particularly when such approximations are used to incorporate new physical effects that may otherwise result in prohibitive computational expense, as well as in scenarios where it may be argued that inertial effects are relatively mild, such as during earthquake nucleation or during aseismic slip transients (Rice, 1993; Segall & Rice, 1995; Liu & Rice, 2005, 2007; Rubin & Ampuero, 2005; Segall et al., 2010; Liu, 2014; Lambert & Barbot, 2016; Erickson et al., 2017; Allison & Dunham, 2018). However, as with all approximations, it is important to be aware of how such simplifications modify the outcome of study (Thomas et al., 2014).

Let us review the quasi-dynamic approximation for inertial effects during sliding and study their implications for the long-term interaction of two fault segments. In the 2D boundary integral formulation, the elastodynamic shear stress along a 1D fault plane, can be expressed as (Cochard & Madariaga, 1994; Perrin et al., 1995):

$$\tau(x,t) = \tau^0(x,t) + \phi_{\text{static}}(x,t) + \phi_{\text{dynamic}}(x,t) - \eta V(x,t), \quad (10)$$

where  $\tau^0(x,t)$  are the "loading" tractions (i.e. the stress induced on the fault plane if it were constrained against any slip),  $\phi_{\text{static}}(x,t)$  and  $\phi_{\text{dynamic}}(x,t)$  represent the static and dynamic contributions to the stress transfer along the fault, respectively, and the last term

344 represents radiation damping ( $\eta = \mu/(2c_s)$  for mode III).

345 The static solution for the equations of motion would only contain  $\phi_{\text{static}}$ , which de-  
 346 pends only on the current values of slip along the fault. However, the static solution does  
 347 not exist during dynamic rupture when inertial effects becomes important.  $\phi_{\text{dynamic}}$  and  $\eta V$   
 348 both arise due to the inertial effects.  $\phi_{\text{dynamic}}$  represents the wave-mediated stress interac-  
 349 tions along the interface and this term is challenging to compute as it requires calculating  
 350 convolutions on time and storing the history of deformation. Radiation damping  $\eta V$  is  
 351 much easier to incorporate as it depends on the current slip rate, and represents part of  
 352 the radiated energy (Rice, 1993). The quasi-dynamic approximation, in which  $\phi_{\text{dynamic}}$  is  
 353 ignored and only  $\eta V$  is included, allows the solution to exist during inertially-controlled dy-  
 354 namic rupture. However, the solution is altered from the true elastodynamic representation.

355 Let us consider the long-term behavior of fault model M1, as examined in section 3,  
 356 but now using the quasi-dynamic approximation. For well-resolved quasi-dynamic simula-  
 357 tions of fault model M1, we find that the long-term slip behavior of the two fault segment  
 358 system is even simpler than for the fully dynamic case, with ruptures being exclusively  
 359 isolated to individual segments and the jump rate being zero (Figure 6A). For simulations  
 360 with the increasing cell size, and thus decreasing spatial resolution, we see increased vari-  
 361 ability in the size of the individual ruptures, to the point where some marginally-resolved  
 362 simulations produce ruptures that jump across the VS barrier, whereas well-resolved simu-  
 363 lations of the same fault model never do (Figure 6B-C). The increasing cell size also leads  
 364 to increased production of smaller events and more complicated fault behavior, similarly to  
 365 the fully dynamic simulations (Figure 6D-F).

366 In addition to substantially reducing the computational expense associated with  
 367 calculating the wave-mediated stress transfers, quasi-dynamic simulations place milder  
 368 constraints on the spatial resolution since the cohesive zone always remains near the quasi-  
 369 static estimate,  $\Lambda \approx \Lambda_0 = \Lambda(v_R = 0^+)$  (Figure 6G-H). This is because the stress transfer  
 370 calculated for the ruptures is always quasi-static, and the much stronger stress transfer  
 371 due to waves is ignored (Figure 7E). As a result, the quasi-dynamic simulations produce  
 372 significantly smaller slip velocities and rupture speeds than the fully dynamic ones 7A-C,  
 373 consistent with previous studies (Lapusta & Liu, 2009; Thomas et al., 2014).

374 One can attempt to enhance the slip rates and rupture speeds in the quasi-dynamic  
 375 simulations by reducing the radiation damping term  $\eta$ ; this can be interpreted as increasing  
 376 the effective shear wave speed in the radiation damping term  $c_s^{\text{enh.}} = \beta c_s$ , thus allowing for  
 377 higher slip rates (Lapusta & Liu, 2009). We compare the enhanced quasi-dynamic simu-  
 378 lations ( $\beta = 3$ ) with the standard quasi-dynamic ( $\beta = 1$ ) and fully dynamic simulations of  
 379 fault model M1 (Supplementary Figure S3). Decreasing the radiation damping increases  
 380 the effective rupture speed and slip rate (Figure 7A -C) in comparison to the standard  
 381 quasi-dynamic simulation, however, for the parameters considered, it does not substantially  
 382 alter the long-term interactions of the two fault segments, nor match the rate of ruptures  
 383 jumping across the VS barrier in the fully dynamic case (Supplementary Figure S3).

384 In comparing the three simulations with different treatment of the inertial effects,  
 385 it is clear that the fully dynamic ruptures result in higher slip rates and narrowing of the  
 386 cohesive zone (Figure 7). For simulations with standard rate-and-state friction, the peak  
 387 shear stresses vary mildly from fully dynamic versus quasi-dynamic representations, as  
 388 they are limited by the shear resistance of the fault, which has a relatively mild logarithmic  
 389 dependence on slip rate. However, the stress transfer along the fault substantially differs  
 390 for fully dynamic versus quasi-dynamic representations (Figure 7E). The difference between  
 391 the stress transfer term and the shear stress is accommodated by the radiation damp-  
 392 ing  $\eta V$ , which results in higher slip rates  $V$  to balance the larger dynamic stress transfers  
 393 (Figure 7C - E). Hence while the resolved peak shear stresses along the fault may be com-  
 394 parable due to the specific choice of the constitutive relationship, the rupture dynamics and  
 395 kinematics, as seen through the stress transfer, slip rate, and rupture speed along the fault,  
 396 differ considerably with and without the inclusion of full inertial effects.

397 These larger dynamic stress transfers facilitate the triggering and continued propa-  
 398 gation of slip on the neighboring fault segment, rather than leaving the rupture to always  
 399 be arrested by the creeping barrier, as in the well-resolved quasi-dynamic simulations  
 400 (Supplementary Figure S3). Decreasing the radiation damping term allows for somewhat  
 401 higher slip rates and arbitrarily higher rupture speeds, but it does not mimic the full effects  
 402 in the dynamic stress transfer, particularly at the rupture front. As the result, the fully  
 403 dynamic simulations have higher jump rates. The differences between fully dynamic and  
 404 quasi-dynamic approximations can be even more substantial for models with enhanced

405 weakening at seismic slip rates from the flash heating of contact asperities or the thermal  
 406 pressurization of pore fluids (Thomas et al., 2014).

## 407 5 Rupture jump rates in simulations with similar 408 power-law frequency-magnitude statistics and 409 earthquake stress drops

410 Two common observations about natural earthquakes and regional seismicity are  
 411 the average static stress drops between 1 to 10 MPa independently of the event magni-  
 412 tude (e.g Allmann & Shearer, 2009; Ye et al., 2016) as well as the frequency-magnitude  
 413 statistics of earthquakes within a region, which commonly follow the Gutenberg-Richter  
 414 power law relation (Field et al., 2013). Some earthquake simulators are capable of matching  
 415 these observations (Shaw et al., 2018). An important question is whether matching these  
 416 constraints allows simulators to be predictive for other quantities of interest to seismic haz-  
 417 ard assessment, such as the probability of multiple fault-segment ruptures, despite using  
 418 approximations for inertial effects and oversized computational cells.

419 Let us consider this question using simulations of earthquake sequences in five fault  
 420 models with the same (simple) fault geometry but different friction properties and different  
 421 assumptions about inertial effects, and one additional model in which the effective seismo-  
 422 genic depth  $\lambda_S$  is slightly reduced from 15 to 14 km (Figure 8, Table 2). All six models  
 423 have comparable nucleation and quasi-static cohesive zone sizes (Table 2) and use oversized  
 424 cells of  $\Delta x = 1000$  m. (An example of well-resolved simulations with similar conclusions is  
 425 given in section 7.) The six simulations produce comparable frequency-magnitude distri-  
 426 butions when interpreted as power-law, characterized by b-values of 0.3-0.4 for 4000 years  
 427 of the simulated time. All six simulations also produce ruptures with comparable average  
 428 static stress drops (Supplementary Figure S4), with values typically between 1 and 10 MPa,  
 429 as commonly inferred for natural earthquakes (Allmann & Shearer, 2009; Ye et al., 2016).

430 However, the probability of a rupture jumping across the VS barrier varies among  
 431 the six simulations, ranging from 0 to near 1. This substantial variability in jump rate for

432 simulations with comparable power-law frequency-magnitude statistics persists in longer-  
433 duration simulations over 20,000 years, where both the 20,000-year jump rate and distribu-  
434 tions of jump rates within individual 2000-year periods can substantially differ (Figure 9).  
435 In particular, fault model M1 results in a jump rate of 0 for the quasi-dynamic simulation  
436 and near 1 for the fully dynamic simulation (Figures 8 and 9A vs. D). This case illustrates  
437 how using approximations for inertial effects may considerably bias estimates of the ac-  
438 tual rate of multi-segment ruptures, even if the power-law frequency-magnitude statistics  
439 and static stress drops are comparable. In addition, the suite of simulations suggest that  
440 the probability of ruptures jumping across the VS barrier is sensitive to variations in the  
441 frictional parameters, effective normal stress, as well as minor changes in the seismogenic  
442 depth.

443 Note that one-segment and two-segment events would not appear that different on  
444 the logarithmic moment-magnitude scale. In our 2D crustal fault model, slip is limited by  
445 the seismogenic thickness, resulting in (geometric) pulse-like rupture propagation for large  
446 events. If one assumes that large ruptures have comparable average slip given the specific  
447 geometry of our simple model, then ruptures that span a single segment or two segments  
448 differ by about a factor of two based on the difference in rupture area. A factor of 2 in  
449 seismic moment changes the moment magnitude  $M_w$  only modestly. For example, a single-  
450 segment rupture with a seismic moment of  $0.5 \times 10^{20}$  Nm corresponds to  $M_w$  7.06 whereas  
451 a two-segment rupture with a seismic moment of  $10^{20}$  Nm corresponds to  $M_w$  7.26; such  
452 moment magnitudes would be binned together for the choice of 0.5 bin width in Figure 8.  
453 Furthermore, the actual amount of slip in individual ruptures can vary; in our simulations,  
454 some single-segment ruptures exhibit greater average slip than two-segment ruptures (Fig-  
455 ure 8), resulting in more variability in seismic moment among large ruptures and greater  
456 overlap in the moment of single and two-segment ruptures. The distinction in the seismic  
457 moment of large single-segment and multi-segment ruptures may be even less obvious in  
458 more realistic models of fault networks with fault segments of varying surface area.

459 The results from our simple 2-D modeling suggest that reproducing static stress  
460 drops and the b-value of the frequency-magnitude event distribution interpreted as a  
461 power-law does not clearly provide sufficient predictive power for rupture jump rates,  
462 although the results could be different for models with additional physics, as further dis-

463 cussed in Section 8. This finding is perhaps not surprising given that many combinations  
464 of rate-and-state properties and effective normal stress may produce ruptures with compa-  
465 rable static stress changes (Supplementary Figure S4), but different overall levels of shear  
466 resistance. Similarly, a number of studies have demonstrated that power-law frequency-  
467 magnitude statistics can be reproduced in many models, including discrete fault models  
468 (Burridge & Knopoff, 1967; Bak & Tang, 1989; Olami et al., 1992), continuum fault models  
469 that are inadequately resolved and therefore numerically discrete (Ben-Zion & Rice, 1995),  
470 continuum models with spatially heterogeneous frictional properties (Hillers et al., 2006,  
471 2007), and continuum models of single or multiple fault segments with larger instability  
472 ratio (Wu & Chen, 2014; Cattania, 2019; Barbot, 2021). Therefore, Gutenberg-Richter  
473 statistics may be compatible with a range of fault properties, and may not pose a consider-  
474 able physical constraint on its own. In particular, the presence of smaller-event complexity  
475 can be due to factors unrelated to the potential for ruptures jumping between segments,  
476 such as small-scale heterogeneity or heterogeneous loading conditions (Rice, 1993; Hillers et  
477 al., 2006, 2007).

478 Note that, while the simulations of Figures 8 and 9 have similar power-law frequency-  
479 magnitude statistics with comparable b-values, the underlying frequency-magnitude dis-  
480 tributions are different, especially for the larger events (Supplementary Figure S5). Some  
481 of these distributions are more consistent with the characteristic-earthquake statistics  
482 suggested by some studies for individual fault segments (Schwartz & Coppersmith, 1984;  
483 Bakun & McEvilly, 1984; Parsons, 2008). Further study is needed to determine whether re-  
484 producing these more detailed frequency-magnitude distributions, especially for the largest  
485 events and perhaps with finer magnitude binning (Supplementary Figure S6), would allow  
486 simulations to capture the rates of single and two-segment ruptures, and how close the  
487 agreement would have to be. However, the practical implications of such a study could be  
488 limited due to limited statistical information about large earthquakes for a given fault net-  
489 work of interest, due to their infrequent occurrence and relatively short periods of reliable  
490 earthquake records.

## 491      6 Resolution and convergence of SEAS simulations of 492      faults with higher instability ratios

493      As discussed in section 3, we find that the discretization required to achieve long-  
494      term numerical convergence in simulations of fault model M1, with instability ratio of  
495       $\lambda_{VW}/h_{RR}^* \approx 21$ , is more stringent than the current standards based on simulations of sin-  
496      gle dynamic ruptures and shorter SEAS simulations with lower instability ratios (Day et  
497      al., 2005; Lapusta & Liu, 2009). It has been demonstrated that fault models with rela-  
498      tively low instability ratios can result in quasi-periodic behavior, as seen in fault model M1  
499      (Figure 2), whereas increasing the instability ratio can lead to more variable sequences of  
500      events with partial-segment ruptures of different rupture size, potentially consistent with  
501      Gutenberg-Richter scaling (e.g Lapusta et al., 2000; Lapusta & Rice, 2003; Wu & Chen,  
502      2014; Michel et al., 2017; Cattania, 2019). As simulations with higher instability ratios can  
503      produce ruptures with a wider variety of rupture sizes, with the rupture size depending on  
504      the prestress conditions before rupture nucleation, one could hypothesize that simulations  
505      of fault models with higher instability ratios may be more sensitive to how the evolution of  
506      shear stress is resolved over long-term fault behavior.

507      To test that, let us consider sequences of events in fault model M5 (Table 2), which  
508      has smaller characteristic slip distance, hence smaller nucleation size ( $h_{RR}^* \approx 603$  m),  
509      and larger instability ratio ( $\lambda_{VW}/h_{RR}^* = 53$  vs. 21 in M1). Interestingly, we find that the  
510      long-term sequence of simulated events in this model is not the same for finely-discretized  
511      simulations with cell sizes of 25, 12.5 and 6.25 m (Figure 10), in which the quasi-static  
512      cohesive zone  $\Lambda_0$  is resolved by 18, 36 and 72 cells, respectively. The simulations produce  
513      nearly identical fault behavior for the first several hundred years of simulated time, but  
514      then eventually begin to differ (Figure 10A-C).

515      Let us consider the first event in the three simulations of model M5 with fine dis-  
516      cretization (Figure 10A-C), which all have the same initial conditions. If we examine the  
517      local evolution of shear stress vs. slip at two spatial points in the simulations, the results  
518      are virtually identical (Supplementary Figure S7A-B), suggesting that a single dynamic  
519      rupture in these finely-discretized simulations is adequately resolved. The evolution of shear  
520      stress and slip rate at the rupture front with time is also well-resolved for each individual

521 simulation. While the different spatial resolutions result in small variations in the timing  
522 and magnitude of the resolved properties at specified locations (Supplementary Figure S7C-  
523 F), these differences are well within of what is considered well-resolved and convergent in  
524 prior studies (e.g Day et al., 2005). Early in the rupture, shortly after nucleation (near  
525  $x = 30$  km), the rupture front is almost identical in the three simulations. (Supplementary  
526 Figure S7C & E). As the rupture continues, small numerical differences for different reso-  
527 lutions result in minor differences in the rupture, such as less than 0.08% difference in the  
528 rupture arrival time and 2% difference in the peak slip rate between the two best-resolved  
529 simulations at the location close to the end of the rupture (Supplementary Figure S7D  
530 & F). Such minor differences arise even for fine resolutions due to cumulative effects of  
531 slightly different representations of the solution by the discrete cells; for example, the fixed  
532 computational cells sample slightly different portions of the passing rupture front, leading  
533 to small accumulating differences in the magnitude of the shear stress and slip rate.

534 These small differences - that do not substantially alter the resulting rupture charac-  
535 teristics of individual events - do eventually alter the resulting earthquake sequences. For  
536 several ruptures early on in finely-discretized simulations, the slip and shear stress distri-  
537 butions before and after individual events are virtually indistinguishable (Figure 11A-B).  
538 However, eventually the small variations accumulate, resulting in enough differences in  
539 prestress conditions to cause more substantial differences in rupture lengths and amounts  
540 of slip within individual events, as well as changes in timing and location of earthquake  
541 nucleations (Figure 11C-E). As a result, the long-term history of sequences of slip events is  
542 altered (Figure 11F), including the rate of ruptures that jump across the VS barrier. We  
543 hypothesize that this alteration occurs for higher but not lower instability ratios due to  
544 more complex earthquake sequences in the latter case, although this issue requires further  
545 study.

546 Despite the specific sequences of events being different in the finely-discretized simu-  
547 lations shown in Figure 10A-C, we do find that certain outcomes are quite similar between  
548 these simulations, such as relationships between average static stress drop and seismic  
549 moment, average slip and rupture length, and breakdown energy and average slip, as well  
550 as general characteristics of the evolution of average shear stress and shear heating with  
551 time (Figure 12). Other parameters, such as the rate of ruptures jumping from one fault

552 segment to another, are sensitive to numerical resolution even in these finely-resolved sim-  
553 ulations, although they have relatively similar values (from 0.64 to 0.78). This highlights  
554 how the criteria for adequate discretization in numerical simulations can depend on both  
555 the physical problem being considered and the outcome of interest. Note that while it is  
556 plausible that further discretization of fault model M5 would result in eventual conver-  
557 gence, and thus potentially a true rate of two-segment ruptures, the spatial discretization  
558 considered in this study is already much finer than those considered in most numerical  
559 SEAS studies, especially in more realistic models of 2D faults in 3D media which are often  
560 challenged to resolve  $\Lambda_0$  by even 3 cells.

561 While the specific rate of ruptures jumping across the VS barrier varies among these  
562 finely-discretized simulations of fault model M5, it is possible that some broader statistical  
563 features of the jump rate are more robust. We examine the frequency-magnitude and 2000-  
564 year jump rate statistics for the long-term sequences of events in simulations of model M5  
565 with different discretization. While the distributions mildly vary among finely-discretized  
566 simulations with differing cell sizes (12.5 m and 25 m), they are comparable (Figure 13  
567 and Supplementary Figure S8). Thus, one can ascertain information about the probabili-  
568 ty distribution for the rate of multi-segment ruptures, even if specific results vary due to  
569 numerical discretization. Such small numerical perturbations could potentially be consid-  
570 ered representative of various sources of physical perturbations on natural faults, and the  
571 statistical consistency of the distributions could be explored by producing ensembles of  
572 simulations with varying initial conditions. However, our results suggest that it is still im-  
573 portant to sufficiently resolve the rupture process as the statistical distributions for rupture  
574 properties in simulations using oversized cells can be more substantially impacted by nu-  
575 matical artifacts and considerably vary from simulations with finer discretization (Figures  
576 13 and 14).

## 577      7 Resolution and convergence in SEAS simulations

## 578      with moderate rupture speeds due to an

## 579      approximation for off-fault plasticity

580      While the 2-D fault models discussed in this study can be considered relatively sim-  
 581      ple, in some ways they can be particularly challenging to resolve. In fault models with  
 582      purely elastic bulk, dynamic ruptures are able to accelerate to rupture speeds close to  
 583      the limiting values  $c_L$  (e.g. Figure 7 for fault model M1), making it difficult to resolve  
 584      the significantly shrinking cohesive zone  $\Lambda$ . For example, during fully dynamic ruptures  
 585      in simulations of fault model M5, the rupture speed approaches  $0.99c_L$  and the cohesive  
 586      zone shrinks more than 7 times to about 63.5 m. In real rocks, high slip rates and hence  
 587      high strain rates associated with dynamic rupture would be mitigated by off-fault inelastic  
 588      behavior around the rupture front, which would contribute to limiting the rupture speed  
 589      (Andrews, 2004; Dunham et al., 2011a).

590      In order to examine how conditions for resolution and convergence may differ in long-  
 591      term SEAS simulations with more moderate rupture speeds, we approximate the effects of  
 592      off-fault yielding by employing a limit on the slip velocity, as suggested by Andrews (2004)  
 593      and discussed in detail in Lambert et al. (2021). Such slip velocity limit is meant to cap-  
 594      ture the effect on rupture propagation of limiting off-fault elastic strains around the rupture  
 595      front, as would be expected with plastic yielding. We consider long-term fully dynamic  
 596      simulations of fault model M5 with the slip velocity limited to 2 m/s in order to maintain  
 597      rupture speeds around  $0.8c_L$ , consistent with the cohesive zone shrinking by about a factor  
 598      of 2 from the quasi-static estimate.

599      Surprisingly, the finely-discretized simulations of fault model M5 with limited rup-  
 600      ture speed still produce differing sequences of events, despite the rupture front and local  
 601      behavior being well-resolved and nearly identical for cell sizes of 6.25 to 25 m (Figure 15  
 602      and Supplementary Figure S9). As with the standard fully dynamic simulations without  
 603      the plasticity approximation, well-resolved simulations of fault model M5 with the velocity  
 604      limit are nearly identical for the initial few sequences (Supplementary Figure S10A-B).  
 605      However, the sequences of events begin to differ due to slight differences in how the evo-

606 lution of shear stress is resolved during a slow-slip transient within the nucleation region  
607 of an impending rupture, resulting in a 3-year delay between the nucleation of the sub-  
608 sequent rupture in each simulation (Supplementary Figure S10C-D). As discussed earlier  
609 for the standard fully dynamic simulations, the small differences in prestress lead to mild  
610 differences in slip and rupture size in subsequent events, which eventually compound to  
611 produce more substantial variations in the long-term sequences of events (Supplementary  
612 Figure S10E-H). These results once again illustrate the extreme sensitivity of the long-term  
613 sequences of events, and rates of two-segment ruptures, in this highly nonlinear problem,  
614 as well as the significance of resolving how aseismic processes load, relax, and redistribute  
615 stress along faults.

616 It is possible that sharp edges in the slip-rate function due to the velocity-limit ap-  
617 proximation for off-fault plasticity may introduce higher-frequency contributions to the  
618 elastic stress interactions that are challenging to resolve. Numerical studies have also  
619 shown that the explicit consideration of off-fault plasticity in numerical earthquake mod-  
620 els requires special consideration; for example, some common plasticity models, such as  
621 rate-independent Drucker-Prager plasticity, can be mathematically ill-posed for some stress  
622 states and require a regularization to determine unique solutions with sufficient numerical  
623 refinement (Rudnicki & Rice, 1975; Andrews, 2005; Dunham et al., 2011a; Erickson et al.,  
624 2017). Thus, while incorporating additional sources of dissipation like off-fault plasticity  
625 may assist in limiting the rupture speed and making the dynamic cohesive zone easier to  
626 resolve, such additional physics may require its own special consideration to achieve numer-  
627 ical convergence. Further investigation of appropriate approximations for off-fault plasticity  
628 and other off-fault behavior using detailed dynamic rupture simulations would facilitate the  
efficient incorporation of such physics into long-term SEAS simulations.

630 Interestingly, we see similar lack of convergence in quasi-dynamic simulations of fault  
631 model M5, where long-term sequences, including the rate of two-segment ruptures, differ  
632 in seemingly well-resolved simulations due to the compounded effects of small numerical  
633 differences (Supplementary Figures S11 and 12). Moreover, despite the rupture front being  
634 better resolved in the quasi-dynamic simulations and in fully dynamic simulations with the  
635 plasticity approximation than in the standard fully dynamic simulations, the sequences of  
636 events begin to diverge earlier. Specifically, while the standard fully dynamic simulations of

637 fault model M5 with cell sizes of  $\Delta x = 6.25$  and  $\Delta x = 12.5$  m have the same event sequences  
638 through approximately 600 to 700 years of simulated time, fully dynamic simulations with  
639 the plasticity approximation begin to substantially differ between 200 to 300 years, and  
640 quasi-dynamic simulations begin to noticeably differ between 100 to 200 years.

641 A potential explanation for this finding is that both the quasi-dynamic approximation  
642 and strong limitation on slip rate for fully dynamic simulations also limit the magnitude  
643 of the stress transfer along the fault (Supplementary Figure S13), making the simulations  
644 more sensitive to small numerical differences. Thus, while the lower stress concentrations  
645 in both cases facilitate maintaining slower ruptures and resolving the breakdown of shear  
646 resistance at the rupture front, the smaller magnitudes for the stress transfer along the  
647 fault makes rupture propagation more sensitive to variations in the pre-existing shear stress  
648 ahead of the rupture front. Note that while the approximation for off-fault plasticity sub-  
649 stantially limits the peak slip rate and magnitude of the stress transfer along the fault, the  
650 overall stress transfer for the fully dynamic rupture including the plasticity approximation  
651 is still more pronounced than that of the quasi-dynamic ruptures, and remains more pro-  
652 nounced well behind the rupture front due to the continued arrival of waves from ongoing  
653 slip in already-ruptured regions. Both the quasi-dynamic simulations and the fully dynamic  
654 simulations with the plasticity approximation produce comparable static stress drops and  
655 frequency-magnitude statistics to the standard fully dynamic simulations (Supplementary  
656 Figures S8, 11 and 14). However, the rupture speeds and rates of two-segment ruptures are  
657 consistently higher for the fully dynamic simulations due to the substantially larger stress  
658 transfer. These results emphasize the significance of inertial effects when considering how  
659 ruptures navigate various forms of fault heterogeneity.

660 The simulations of model M5, without and with the plasticity approximation, provide  
661 another example of how earthquake sequences with similar frequency-magnitude statistics  
662 can result in different jump rates across the velocity-strengthening barrier. While the sim-  
663 ulations with cell sizes of 6.25, 12.5, and 25 m have well-resolved cohesive zones (Figures  
664 10 and 15) and similar event statistics (Supplementary Figures S8 and S14), they have  
665 jump rates ranging from 0.7-0.8 without the plasticity approximation to 0.3-0.5 with the  
666 plasticity approximation (Figures 10 and 15).

## 667 8 Conclusions and Discussion

668 We have investigated the sensitivity of numerical simulations of long-term sequences  
 669 of earthquakes and aseismic slip (SEAS) to numerical discretization and treatment of iner-  
 670 tial effects, using a simplified 2-D model of a 1D fault with two co-planar seismogenic, VW  
 671 segments separated by a VS barrier. Our focus is, in part, on the resulting rate of rupture  
 672 jumps across the barrier.

673 We find that the convergence of long-term simulated earthquake sequences with  
 674 increasing numerical resolution may not always be achievable, at least practically given cur-  
 675 rent computational capabilities. Even if simulations are sufficiently discretized to produce  
 676 consistent modeling results for individual ruptures or short sequences of events, they can  
 677 still produce different long-term sequences due to compounded effects of small numerical  
 678 differences over many events. We have achieved the convergence for fault models with lower  
 679 instability ratios  $\lambda_{VW}/h_{RR}^*$ , i.e., lower fault lengths in comparison to the nucleation size  
 680 (Figure 3). In contrast, models with higher instability ratios exhibit different long-term  
 681 behavior even in simulations that are well discretized by standard metrics (Day et al., 2005;  
 682 Lapusta & Liu, 2009), including different specific sequences of earthquakes and different  
 683 probability of ruptures jumping across the VS barrier. In the cases with convergent long-  
 684 term behavior, the criteria for numerical resolution that leads to the same evolution of slip  
 685 are more stringent than those for individual dynamic ruptures, i.e., the dynamic cohesive  
 686 zone size needs to be discretized by more cells.

687 Our results show that numerical convergence in SEAS simulations depends not only  
 688 on how well important length-scales are discretized but also on the sensitivity of the spe-  
 689 cific physical problem to small numerical perturbations. In particular, our results suggest  
 690 that faults with higher instability ratios are more sensitive to accumulating numerical per-  
 691 turbations (Figure 16), although that conclusion is reached here for simulations governed  
 692 by only standard rate-and-state friction and requires further study in models with differen-  
 693 t/additional fault physics. While quasi-dynamic simulations are easier to resolve and thus  
 694 should result in smaller numerical discrepancies for sufficiently small cell sizes, the milder  
 695 stress transfer compared to fully dynamic ruptures can make long-term quasi-dynamic  
 696 simulations more sensitive to small perturbations in shear stress, as occurs in fault model

M5. In contrast, while earthquake sequence simulations including enhanced dynamic weakening can require finer discretization to resolve the rapid weakening rates at the rupture front compared to standard rate-and-state friction, the larger dynamic stress changes in fault models with more efficient weakening can make rupture propagation less sensitive to different levels of fault heterogeneity, promoting the propagation of predominantly larger ruptures and hence resulting in relatively simple earthquake sequences even for models with high instability ratios (Lambert et al., 2021, in review). Hence empirical discretization criteria, such as those of (Day et al., 2005), should be seen as guidelines that may not be universally applicable to all physical models and outcomes of interest. Moreover, for some models, here is the possibility that numerical convergence of long-term slip may not be achievable, though statistical consistency may hold for some modeling results but not others (Figure 16).

For the fault models considered, we find that the specific sequences of slip events and rate of earthquake ruptures jumping across a VS barrier are sensitive to the numerical resolution, representation of inertial effects, as well as minor changes in physical properties, such frictional parameters, confining stress, seismogenic depth, and barrier size. This suggests that, at least in this relatively simple model, the rate of ruptures jumping across a VS barrier is not a stable outcome that can always be reliably estimated from numerical simulations, unless the barrier is so large or small that the rate is reliably zero or 1 (Figure 17). The sensitivity of the specific timing and sequences of slip events in models with higher instability ratios is suggestive of deterministically chaotic long-term fault behavior, as has been suggested by theoretical studies of coupled spring-sliders and continuum models with increasing instability ratios (Huang & Turcotte, 1990; N. Kato, 2014; Barbot, 2019). The sensitivity of rupture jump rates to small changes in our models suggests that the jump rates across barriers that serve as earthquake gates may also be highly sensitive to small physical perturbations on natural faults, and thus may be impractical to estimate in a reliable manner.

However, even for the models that do not achieve deterministic convergence with finer resolution, we find that some characteristics of well-resolved simulations are preserved, qualitatively and quantitatively. The characteristics include ranges of average source properties such as the average static stress drop, quantities related to energy partitioning such

as the average breakdown energy, as well as general features of the average shear stress and shear heating evolution throughout time (Figure 12). These results suggest that some aspects of physical systems may be reliably determined from a given physics-based model, while others perhaps cannot, in the sense that they are very sensitive to numerical procedures and initial conditions, and even well-resolved models produce different outcomes with respect to those quantities. Our findings also suggest that it may be possible to discern some statistical aspects of the probability distribution for multi-segment ruptures from well-formulated numerical models, even if they do not exhibit convergence of long-term behavior with numerical resolution. However, as the jump rate appears to be sensitive to small perturbations in numerical and physical properties, it would be prudent to examine the statistical consistency of the jump rate distribution through large ensembles of models, particularly given the uncertainty in values for physical model parameters. Another route for examining plausible rupture scenarios for large earthquakes navigating key sections of fault networks would be to conduct detailed dynamic rupture simulations that can handle more realistic fault geometries with full treatment of inertial effects (e.g Wollherr et al., 2019; Ulrich et al., 2019), and produce large ensembles of dynamic rupture scenarios with variations in initial conditions inspired by SEAS simulations.

Our results confirm that quasi-dynamic simulations that ignore wave-mediated stress transfer during dynamic rupture can lead to qualitative differences in the resolved rupture behavior and long-term sequences of slip events. The wave-mediated stress redistribution not only facilitates long-range interactions among portions of a fault and neighboring segments, but also alters the state of stress at the rupture front, promoting higher slip rates and more focused stress concentrations. In particular, the relatively small static stress transfer in quasi-dynamic simulations makes the rupture front more susceptible to unfavorable conditions, such as those one may expect from frictional heterogeneity, fault roughness, and regions of unfavorably low prestress. In contrast, the larger wave-mediated dynamic stresses in fully dynamic ruptures may assist rupture propagation in navigating unfavorable fault conditions and geometric irregularities (Harris et al., 1991; Harris & Day, 1993, 1999; Kame et al., 2003; Duan & Oglesby, 2006; Dunham et al., 2011b; Galvez et al., 2014; Thomas et al., 2014; Douilly et al., 2015; Lozos et al., 2015; Withers et al., 2018; Ando & Kaneko, 2018; Wollherr et al., 2019; Ulrich et al., 2019). Moreover, the spatial pattern for

dynamic stresses, which affects the preferential direction for ruptures to branch or jump to neighboring faults, rotates as a function of the rupture speed, and hence can be considerably different from a quasi-dynamic rupture (Kame et al., 2003). Thus, considering full inertial effects during individual dynamic ruptures and long-term sequences of slip events is particularly important when considering the interaction of multiple fault segments and the likelihood of ruptures propagating through fault portions with potentially unfavorable conditions.

Our results also confirm that using increasingly oversized cells, with or without wave-mediated stress transfers, results in a progressively more complex slip response, with broader distributions of event sizes, consistent with conclusions from prior studies (Benzion & Rice, 1995). Using oversized cells and/or ignoring wave-mediated stress transfer significantly modifies the probability of two-segment ruptures, as well as the resulting earthquakes sequences.

Finally, we find that simulations with similar b-values of the cumulative frequency-magnitude statistics and similar average static stress drops can have substantially different rates of ruptures that jump between two segments. We caution that models with more realistic geometry and/or additional physics may behave differently; for example, more realistic non-planar fault geometry or enhanced dynamic weakening may dominate the model outcomes (e.g., the rupture jump rates) to the point of making them insensitive to certain variations in model assumptions or parameters. However, our findings suggest that such insensitivity of model outcomes cannot be assumed and needs to be established through suites of simulations with different plausible properties and assumptions.

In order to constrain the most relevant fault physics and property ranges, and hence to maximize the predictive power of numerical earthquake models for future fault behavior, numerical simulations of fault models can explore how choices in physical mechanisms and conditions are reflected in a range of observations taken together, including, but not limited to, geodetic observations of interseismic and postseismic motions (e.g. Barbot et al., 2012), geological records of past earthquakes (e.g. Sieh, 1978; Biasi & Wesnousky, 2017), heat flow constraints (e.g Henyey & Wasserburg, 1971; Lachenbruch & Sass, 1980; Fulton et al., 2013), and seismologically determined properties of earthquakes such as average static stress drops, radiated energy, and the inferred increase in average breakdown en-

790 ergy with rupture size (Abercrombie & Rice, 2005; Rice, 2006; Viesca & Garagash, 2015;  
791 Perry et al., 2020; Lambert et al., 2021). As modeling capabilities continue to develop and  
792 capture realistic fault geometries tailored for specific fault segments, such models can also  
793 aim to reproduce details of more local seismicity patterns, including the interplay between  
794 earthquakes and slow-slip transients (e.g. Ito et al., 2013; A. Kato et al., 2012; Ruiz et al.,  
795 2014), repeating earthquakes (e.g. Chen & Lapusta, 2009; Mele Veedu & Barbot, 2016),  
796 seismic swarm activity, (e.g. Ross et al., 2020), and spatio-temporal variations in frequency-  
797 magnitude statistics (Schorlemmer & Wiemer, 2005; Ishibe & Shimazaki, 2012). While the  
798 frequency-magnitude distribution of seismicity over broad regions like California are gener-  
799 ally consistent with Gutenberg-Richter scaling with typical b-values near unity (Field et al.,  
800 2013), it remains a topic of active debate as to whether such scaling applies to individual  
801 fault segments and their immediate surroundings (Schwartz & Coppersmith, 1984; Wes-  
802 nousky, 1994; Stirling et al., 1996; Ishibe & Shimazaki, 2012; Kagan et al., 2012; Page &  
803 Felzer, 2015; Page & van der Elst, 2018; Field et al., 2017). In particular, some segments of  
804 major mature faults, such as the Cholame and Carrizo segments of the San Andreas Fault,  
805 exhibit notable deviations from typical Gutenberg-Richter scaling and are nearly absent  
806 of microseismicity (Sieh, 1978; Wesnousky, 1994; Bouchon & Karabulut, 2008; Hauksson  
807 et al., 2012; Jiang & Lapusta, 2016; Michailos et al., 2019). Determining plausible phys-  
808 ical conditions compatible with seismicity patterns on such large mature fault segments,  
809 including observed seismic quiescence, is of particular importance for seismic hazard assess-  
810 ment, since the segments have historically hosted some of the largest recorded continental  
811 earthquakes.

812 Such physics-based modeling can then inform laboratory and observational scientists  
813 about the most strategic measurements that can improve constraints on plausible mod-  
814 els and help assess the resolution and sources of potential bias in geophysical inferences  
815 (e.g. Noda et al., 2013; Lin & Lapusta, 2018; Abercrombie, 2021). Note that a number of  
816 physical properties not included in our simplified 2-D models may qualitatively alter the  
817 behavior and hence interaction of neighboring fault segments, such as the explicit consid-  
818 eration of depth variations in slip and the depth extent to which ruptures propagate (e.g.  
819 Jiang & Lapusta, 2016; Wollherr et al., 2019; Ulrich et al., 2019), time-dependent varia-  
820 tions in loading from distributed deformation at depth (Lambert & Barbot, 2016; Allison &

**Figure 1.** Schematic of a strike-slip fault with two co-planar velocity-weakening fault segments separated by a velocity-strengthening barrier. In our simulations, we use a 2D approximation of the problem with a 1D along-strike depth-averaged fault, in which the fault is assumed to be creeping at the loading plate rate  $V_{pl}=10^{-9}$  m/s below the depth of  $\lambda_S=15$  km.

Dunham, 2018), enhanced dynamic weakening at seismic slip rates (Tullis, 2007; Di Toro et al., 2011; Dunham et al., 2011b; Noda & Lapusta, 2013; Perry et al., 2020; Lambert et al., 2021), evolving damage and fault geometry (Lyakhovsky & Ben-Zion, 2009, 2014; Okubo et al., 2019), especially near fault junctions, and hydromechanical coupling due to poroelasticity, fault-zone dilatancy and other fluid effects (Segall & Rice, 1995; Dunham & Rice, 2008; Zhu et al., 2020). These are just a few physical ingredients that merit detailed study in the long-term interaction of fault segments.

Overall, our findings highlight the importance for numerical studies to examine the sensitivity of their outcomes of interest to variations in their modeling parameters, particularly when assessing their predictive value for seismic hazard assessment. Community initiatives, such as the Southern California Earthquake Center (SCEC) code comparisons for dynamic rupture simulations and simulations of sequences of seismic and aseismic slip (Harris et al., 2009; Barall & Harris, 2014; Harris et al., 2018; Erickson et al., 2020), can provide further insight into how numerically-derived results for different physical quantities may depend on numerical methodologies and computational practices. The significant sensitivity of the rate of multi-segment ruptures to small changes in our numerical models implies that this hazard parameter may also be sensitive to physical perturbations on natural faults. This consideration motivates further evaluation of metrics for describing long-term fault behavior and assessing seismic hazard, tasks for which physics-based modeling is well-suited.

Parameter	Symbol	Value
Loading slip rate	$V_{pl}$	$10^{-9}$ m/s
Shear wave speed	$c_s$	3299 m/s
Shear modulus	$\mu$	36 GPa
Poisson's ratio	$\nu$	0.25
Rate-and-state parameters		
Reference friction coefficient	$f_*$	0.6
Reference slip velocity	$V_*$	$10^{-6}$ m/s
Direct effect (VS)	$a_{VS}$	0.02
Evolution effect (VS)	$b_{VS}$	0.003
Direct effect (barrier)	$a_B$	0.05
Evolution effect (barrier)	$b_B$	0.001
Length scales		
Fault length	$\lambda$	280 km
Frictional domain	$\lambda_{fr}$	258 km
Each VW segment	$\lambda_{VW}$	32 km
VS Barrier	$\lambda_B$	2 km
Seismogenic depth	$\lambda_S$	15 km

**Table 1.** Parameter values that are the same in different fault models unless specified otherwise

Parameter	Symbol	M1	M2	M3	M4	M5
Effective normal stress	$\bar{\sigma} = (\sigma - p)$	50 MPa	60 MPa	40 MPa	30 MPa	50 MPa
Characteristic slip	$D_{RS}$	20 mm	20 mm	20 mm	18 mm	8 mm
Direct effect (VW)	$a_{VW}$	0.005	0.005	0.005	0.005	0.005
Evolution effect (VW)	$b_{VW}$	0.015	0.0135	0.0175	0.02	0.015
Length scales						
Quasi-static cohesive zone	$\Lambda_0$	1.1 km	1.0 km	1.2 km	1.3 km	452 m
Nucleation size (R.&A., 2005)	$h_{RA}^*$	1.8 km	1.9 km	1.7 km	1.6 km	733 m
Nucleation size (R.&R., 1983)	$h_{RR}^*$	1.5 km	1.5 km	1.5 km	1.6 km	603 m
Instability ratio	$\lambda_{VW}/h_{RA}^*$	18	17	19	20	44
Instability ratio	$\lambda_{VW}/h_{RR}^*$	21	22	21	21	53

**Table 2.** Parameters values that vary among fault models

**Figure 2.** Interaction of two co-planar fault segments in well-resolved simulations of model M1 demonstrating convergence of simulated earthquake sequences. (A-B) History of cumulative slip over 4000 years in well-resolved fully-dynamic simulations of fault model M1 with initial conditions S1 using (A) 12.5-m and (B) 25-m cell size. Contours for seismic slip are plotted every 0.5 s, with ruptures that jump across the VS barrier colored blue. The simulated fault behavior is virtually indistinguishable between the two resolutions. (C) Frequency-magnitude histograms of events, on top of each other for the two resolutions. The well-resolved simulations produce the same relatively simple and quasi-periodic behavior. (D-E) The evolution of local shear stress and slip velocity at a point ( $x = -20.5$  km, shown by star in A and B), practically indistinguishable even after over 3800 years of simulated time. (F-H) Spatial distribution of shear stress at the rupture front for three locations ( $x = -20$  km, 5 km and 20km) throughout the first rupture in (A-B). While the quasi-static estimate of the cohesive zone  $\Lambda_0$  is about 1.1 km, the actual size of the cohesive zone varies with the local rupture speed throughout the rupture. In these well-resolved simulations, the cohesive zone is always resolved by at least 10 cells.

**Figure 3.** Convergence of well-resolved simulated earthquake sequences in model M1 for longer-term simulations and different initial conditions. (A-B) Cumulative slip over 0-4000 years and 16,000-20,000 years in two well-resolved fully-dynamic simulations of fault model M1 with two different initial conditions, S1 and S2. Contours of seismic slip are plotted every 0.5 s with ruptures that jump across the VS barrier colored blue. The quasi-periodic behavior seen in the first 4000 years in well-resolved simulations, including the rate of ruptures jumping across the VS barrier, remains generally consistent throughout longer-term simulations over 20,000 years (Right). Simulations using different initial shear stress conditions produce different initial sequences of events, however, the simulated sequences converge to the same slip behavior and have the same long-term rates of two-segment ruptures (0.50 over 2,000-20,000 years). (C-D) Normalized frequency-magnitude histograms for events from (A) and (B), respectively, over 4000 and 20,000 years, illustrating that the population statistics in this relatively simple system is the same, apart from the initial start-up period.

**Figure 4.** Less well-resolved simulations of fault model M1 exhibiting different simulated earthquake sequences and rates of two-segment ruptures. (A-B) History of cumulative slip over 4000 years in fully dynamic simulations of fault model M1 using marginal and oversized cells of (A) 125 m and (B) 250 m, respectively. Contours of seismic slip are plotted every 0.5 s, with ruptures that jump across the VS barrier colored blue. (C) Spatial distribution of shear stress around the rupture front in a well-resolved simulation ( $\Delta x = 25$  m, red) and the two simulations with larger cells ( $\Delta x = 125$  and 250 m). As the cell size increases, the resolution of the shear stress evolution at the rupture front decreases, although the resolution would be acceptable in simulations of single ruptures (Day et al., 2005). (D-E) Frequency-magnitude histograms for events in (A-B), respectively. The simulations with larger cells exhibit different long-term sequences of events compared to the well-resolved simulations (Fig. 2C), with increased production of small events and significantly different rates of two-segment ruptures.

**Figure 5.** (A-J) Frequency-magnitude (left) and jump-rate (right) statistics for 20,000 years of simulated earthquake sequences in model M1 with different initial conditions and cell sizes. (A-B) Well-resolved simulations with different initial shear stress conditions result in comparable long-term quasi-periodic sequences, and thus comparable frequency-magnitude statistics and 2000-year jump rate statistics that are generally consistent with the 20,000-year jump rate of 0.50. (C-J) As the resolution decreases, the sequences become more complex with greater variability of event sizes and increased production of smaller events. The jump rate during different 2000-year periods also becomes more variable and can considerably differ from the true jump rate of 0.5 in the well-resolved cases.

**Figure 6.** Interaction of two co-planar fault segments in quasi-dynamic simulations of fault model M1 with varying discretization. (A-C) History of cumulative slip over 4000 years in quasi-dynamic simulations of fault model M1 with initial conditions S1 using (A) adequate discretization, (B) marginal discretization, and (C) oversized cells. Contours of seismic slip are plotted every 0.5 s, with ruptures that jump across the VS barrier colored blue. (D-F) Frequency-magnitude histograms for events in (A-C). (G-H) Spatial distribution of shear stress illustrating the breakdown of shear resistance at the rupture front during quasi-dynamic simulations in fault model M1 with varying spatial resolution. The cohesive zone does not shrink during quasi-dynamic ruptures. A well-resolved rupture front is shown in red with a cell size of 25 m. The cohesive zone ( $\Lambda_0 = 1.1$  km) is resolved by at best 1 to 2 cells for cell sizes of 500 to 1000 m.

**Figure 7.** Comparison of local slip rate, shear stress, and rupture speed for simulations with different treatment of inertial effects. (A) Spatial distribution of slip rate at three instances of time during the first rupture with the same initial conditions in fully dynamic (black), quasi-dynamic (red) and enhanced quasi-dynamic (blue) simulations of fault model M1. (B) The fully dynamic rupture accelerates to a rupture speed close to the limiting wave speed of  $c_L \approx 4.4$  km/s throughout the rupture, whereas the quasi-dynamic ruptures maintain lower effective rupture speeds. Decreasing the radiation damping term for quasi-dynamic ruptures increases the slip rate and rupture speed, but does not truly mimic the acceleration of the fully dynamic rupture. (C-D) A closer look at the spatial distribution of (C) slip velocity and (D) shear stress at a given time highlights how full consideration of inertial effects leads to much higher slip velocities and a more localized stress concentration at the rupture front, which facilitates rupture propagation. Enhancing the quasi-dynamic ruptures with lower radiation damping increases the slip rate but maintains the same quasi-static spatial pattern of stress at the rupture front. (E) The corresponding values of the stress transfer functional near the rupture front. The radiation damping approximation of the inertial effects results in dramatically reduced stress transfer along the fault. The larger total stress transfer in the fully dynamic simulations is balanced by higher slip rates, as shown in (C).

**Figure 8.** Models with comparable power-law frequency-magnitude statistics and static stress drops but very different rate of two-segment ruptures. (A-F) Cumulative frequency-magnitude histograms (top) and history of cumulative slip (bottom) over 4000 years in (A-C) fully dynamic and (D-F) quasi-dynamic SEAS simulations. Contours for seismic slip are plotted every 0.5 s, with ruptures that jump across the VS barrier colored blue. The simulations assume different physical conditions described in the text. All six simulations produce comparable average static stress drops (Supplementary Figure S4) and comparable population statistics with a b-value around 0.33. However, the rate of two-segment ruptures varies from 0 to 1.

**Figure 9.** Variability of jump rates in models with comparable frequency-magnitude statistics and static stress drops. (A-F) Cumulative frequency-magnitude histograms (Top) and normalized 2000-year jump rate histograms (Bottom) over 20,000 years in (A-C) fully dynamic and (D-F) quasi-dynamic SEAS simulations, as shown in Figure 8. The six simulations have comparable frequency-magnitude statistics but the 20,000-year rate of two-segment ruptures varies from 0 to 0.91. The distribution of 2000-year jump rates is also highly variable among the six simulations.

**Figure 10.** Sequences of earthquakes and rates of two-segment ruptures over 4000 years in fully dynamic simulations with different resolution of fault model M5 with higher instability ratio. Seismic slip is contoured every 0.5 s with ruptures jumping across the VS barrier colored blue. (A-C) Slip history for increasingly better-discretized simulations. While the initial 1000 years of simulated behavior appear well resolved and comparable, longer-term simulations begin to diverge due to the compounded effects of small numerical differences, leading to similar but inconsistent jump rates across the barrier. (D-E) The spatial distribution of shear stress at the rupture front. For well-resolved simulations (D), the cohesive zone is resolved by several cells, but is resolved by less than even one cell for poorly-resolved simulations (E). (F-G) Simulations with decreasing numerical resolution can exhibit additional artificial complexity and substantially different long-term fault behavior, including different rates of two-segment ruptures.

**Figure 11.** Compounded effects of minor numerical differences in well-resolved simulations of model M5 result in diverging long-term earthquake sequences. Comparison of the prestress before rupture (left) and resulting slip distributions (right) for several events over the first 1000 years of simulated time in two fully dynamic simulations of fault model M5 using cell sizes of 6.25 m (red) and 12.5 m (black). (A & B) The evolution of shear stress and accumulation of slip during the first few hundred years of simulated time are virtually identical. (C-E) Eventually, small differences in shear stress before events build up due to different numerical approximations, resulting in small differences in slip and rupture length for individual events, as well as the location and timing for the nucleation of smaller events. (F & G) The differences in shear stress accumulate over sequences of events, resulting in noticeable variations of slip in larger events after 800 years of simulated time and, eventually, different histories of large segment-spanning events between the two well-resolved simulations, as shown in Figure 10.

**Figure 12.** Averaged source properties and fault behavior that are generally consistent among well-resolved fully dynamic simulations of fault model M5, despite lack of convergence of slip with finer resolution. (A) Spatially-averaged stress drop versus moment. (B) Average slip versus rupture length. (C) Energy-based average stress drop versus moment. (D) Average breakdown energy versus average slip. (E) Evolution of average shear stress and the shear stress associated with shear heating over 4000 years of simulated sequences of earthquakes. It is apparent that the timing and degree of slip of individual events in the sequences of earthquakes differ. However the general characteristics of the overall average stress evolution, in terms of the maximum and minimum stresses and the average stress drops, are comparable, resulting in virtually indistinguishable shear heating stresses.

**Figure 13.** Different frequency-magnitude and jump rate statistics for 20,000 years of sequences of earthquakes in fully dynamic simulations of fault model M5 with varying cell sizes. (A-F) Frequency-magnitude histograms (Top) and normalized 2000-year jump rate histograms (Bottom) for 20,000 years of simulated SEAS. (A-B) Even well-resolved simulations exhibit mild differences in long-term event statistics, though the frequency-magnitude histograms are similar. The 2000-year jump rate histograms are different but comparable for well-resolved simulations, with the 20,000-year jump rate varying by approximately 15% among the three simulations. (C-F) Simulations with marginal or inadequate resolution have enhanced production of smaller events, as small groups of cells nucleate into ruptures but fail to propagate substantially due to poorly resolved stress concentration at the rupture front. The 20,000-year jump rates and 2000-year jump rate distributions substantially vary for simulations using oversized cells compared to the well-resolved simulations.

**Figure 14.** Scaling of average slip and stress drop with rupture size for numerically-discrete versus well-resolved ruptures in fault model M5. (A-B) Despite different long-term sequences of events, two well-resolved simulations of fault model M5, with cell sizes  $\Delta x = 6.25$  m and  $\Delta x = 12.5$  m, have similar scaling of average slip and static stress drop with rupture size. Simulations using oversized cells produce small numerically-discrete ruptures consisting of only a few cells that fail to propagate due to the poorly resolved stress concentration of the shear stress at the (diffuse) rupture front. This causes large ruptures to occur in poorly-resolved simulations for higher values of shear stress, resulting in large ruptures having greater average slip than in well-resolved simulations (A). The small numerically-discrete ruptures produce variable amounts of slip, despite being restricted to the same rupture size of only 1 to several cells (A), leading to large, upward-sweeping trends in average stress drop with moment, which are purely numerical (B).

**Figure 15.** Sequences of earthquakes and rate of two-segment ruptures over 4000 years in fully dynamic simulations with different resolution of fault model M5 and an approximation of off-fault plasticity. The rupture speed reduces to  $0.8 c_L$  due to the approximation using a velocity limit of  $V_{\text{lim}} = 2$  m/s. Seismic slip is contoured every 0.5 s with ruptures jumping across the VS barrier colored blue. (A-C) Slip history for increasingly well-resolved simulations. The initial few sequences of events appear comparable among well-resolved simulations, however the sequences begin to differ due to the compounded effects of small numerical differences. (D-E) The cohesive zone shrinks by only about a factor of two for rupture speeds below  $0.8 c_L$ , so the rupture front is very well-resolved. (F-G) Simulations with decreasing numerical resolution exhibit additional artificial complexity and substantially different long-term fault behavior, including rates of two-segment ruptures.

Accepted Article

**Figure 16.** Conceptual diagram illustrating potentially convergent versus divergent numerical behavior depending on resolution and model complexity, parameterized by the instability ratio as an example. Well-resolved fault models with low enough instability ratio may potentially be numerically deterministic where adequate discretization results in virtually indistinguishable numerical outcomes. Fault models with higher instability ratio may either have more stringent requirements for numerical discretization in order to achieve long-term convergence, or such convergence may be impossible; either way, achieving numerical convergence in simulations of sufficiently complex fault models, such as with higher instability ratios, would be impractical. In such cases, it may still be possible to achieve statistical consistency among some outcomes within well-resolved simulations, though other properties of the system may be highly sensitive to numerical precision and considerably vary depending on the numerical procedures.

**Figure 17.** Consistent isolation of ruptures on fault segments separated by a larger velocity-strengthening barrier in simulations with adequate discretization and oversized cells. History of cumulative slip over 4000 years in two fully dynamic simulations of fault model M1 that utilize (A) cells that adequately resolve the cohesive zone ( $\Delta x = 25$  m) and (B) oversized cells ( $\Delta x = 1000$  m). Seismic slip is contoured every 0.5 s. The VS barrier is increased in width to 10 km such that ruptures are isolated to individual fault segments in both simulations.

## 841 Acknowledgments

842 This study was supported by the National Science Foundation (grants EAR 1142183 and  
 843 1520907) and the Southern California Earthquake Center (SCEC), contribution No. 10089.  
 844 SCEC is funded by NSF Cooperative Agreement EAR-1033462 and USGS Cooperative  
 845 Agreement G12AC20038. Numerical simulations for this study were carried out on the  
 846 High Performance Computing Center cluster of the California Institute of Technology. This  
 847 study was motivated by insightful discussions within the SCEC community. Details about  
 848 the fault models and numerical parameters for calculations are provided in the main and  
 849 supplementary text, and Tables 1-2. Data were not used, nor created for this research.

## 850 References

- 851 Abercrombie, R. E. (2021). Resolution and uncertainties in estimates of earthquake  
 852 stress drop and energy release. *Philosophical Transactions of the Royal Society*  
 853 *A: Mathematical, Physical and Engineering Sciences*, 379(2196), 20200131.  
 854 doi: 10.1098/rsta.2020.0131
- 855 Abercrombie, R. E., & Rice, J. R. (2005). Can observations of earthquake scal-  
 856 ing constrain slip weakening? *Geophysical Journal International*, 162, 406-424.  
 857 doi: 10.1111/j.1365-246X.2005.02579.x
- 858 Allison, K. L., & Dunham, E. M. (2018). Earthquake cycle simulations with rate-  
 859 and-state friction and power-law viscoelasticity. *Tectonophysics*, 733, 232 -  
 860 256. doi: 10.1016/j.tecto.2017.10.021
- 861 Allmann, B. P., & Shearer, P. M. (2009). Global variations of stress drop for mod-  
 862 erate to large earthquakes. *Journal of Geophysical Research: Solid Earth*,  
 863 114(B1). doi: 10.1029/2008JB005821
- 864 Ando, R., & Kaneko, Y. (2018). Dynamic rupture simulation reproduces spon-  
 865 taneous multifault rupture and arrest during the 2016 Mw 7.9 Kaikoura  
 866 earthquake. *Geophysical Research Letters*, 45(23), 12,875-12,883. doi:  
 867 10.1029/2018GL080550

- 868 Andrews, D. J. (2004, 06). Rupture Models with Dynamically Determined Break-  
869 down Displacement. *Bulletin of the Seismological Society of America*, 94(3),  
870 769-775. doi: 10.1785/0120030142
- 871 Andrews, D. J. (2005). Rupture dynamics with energy loss outside the slip zone.  
872 *Journal of Geophysical Research*, 110. doi: 10.1029/2004JB003191
- 873 Bak, P., & Tang, C. (1989). Earthquakes as a self-organized critical phenomenon.  
874 *Journal of Geophysical Research: Solid Earth*, 94(B11), 15635-15637. doi: 10  
875 .1029/JB094iB11p15635
- 876 Bakun, W. H., & McEvilly, T. V. (1984). Recurrence models and parkfield, califor-  
877 nia, earthquakes. *Journal of Geophysical Research: Solid Earth*, 89(B5), 3051-  
878 3058. doi: <https://doi.org/10.1029/JB089iB05p03051>
- 879 Barall, M., & Harris, R. A. (2014, 11). Metrics for Comparing Dynamic Earthquake  
880 Rupture Simulations. *Seismological Research Letters*, 86(1), 223-235. doi: 10  
881 .1785/0220140122
- 882 Barbot, S. (2019). Slow-slip, slow earthquakes, period-two cycles, full and partial  
883 ruptures, and deterministic chaos in a single asperity fault. *Tectonophysics*,  
884 768, 228171. doi: <https://doi.org/10.1016/j.tecto.2019.228171>
- 885 Barbot, S. (2021). A Spectral Boundary Integral Method for Quasi-Dynamic Rup-  
886 tures of Multiple Parallel Faults. *Bulletin of the Seismological Society of Amer-*  
887 *ica*, 111(3), 1614-1630. doi: 10.1785/0120210004
- 888 Barbot, S., Lapusta, N., & Avouac, J.-P. (2012). Under the hood of the earthquake  
889 machine: Toward predictive modeling of the seismic cycle. *Science*, 336(6082),  
890 707-710.
- 891 Ben-Zion, Y., & Rice, J. R. (1995). Slip patterns and earthquake populations along  
892 different classes of faults in elastic solids. *Journal of Geophysical Research:*  
893 *Solid Earth*, 100(B7), 12959-12983. doi: 10.1029/94JB03037
- 894 Ben-Zion, Y., & Rice, J. R. (1997). Dynamic simulations of slip on a smooth fault in  
895 an elastic solid. *Journal of Geophysical Research: Solid Earth*, 102(B8), 17771-

- 896 17784. doi: 10.1029/97JB01341
- 897 Biasi, G. P., & Wesnousky, S. G. (2017). Bends and ends of surface ruptures.
- 898 *Bulletin of the Seismological Society of America*, 107, 2543-2560. doi:  
899 10.1785/0120160292
- 900 Biasi, G. P., & Wesnousky, S. G. (2021). Rupture passing probabilities at fault  
901 bends and steps, with application to rupture length probabilities for earth-  
902 quake early warning. *Bulletin of the Seismological Society of America*, 111,  
903 2235-2247. doi: 10.1785/0120200370
- 904 Bouchon, M., & Karabulut, H. (2008). The aftershock signature of supershear earth-  
905 quakes. *Science*, 320(5881), 1323–1325. doi: 10.1126/science.1155030
- 906 Burridge, R., & Knopoff, L. (1967). Model and theoretical seismicity. *Bulletin of the*  
907 *Seismological Society of America*, 57(3), 341-371.
- 908 Cattania, C. (2019). Complex earthquake sequences on simple faults. *Geophysical*  
909 *Research Letters*, 46(17-18), 10384-10393. doi: 10.1029/2019GL083628
- 910 Chen, T., & Lapusta, N. (2009). Scaling of small repeating earthquakes explained by  
911 interaction of seismic and aseismic slip in a rate and state fault model. *Journal*  
912 *of Geophysical Research*, 114. doi: 10.1029/2008JB005749
- 913 Cochard, A., & Madariaga, R. (1994). Dynamic faulting under rate-dependent fric-  
914 tion. *Pure and Applied Geophysics*, 142, 419-445. doi: 10.1007/BF00876049
- 915 Day, S. M., Dalguer, L. A., Lapusta, N., & Liu, Y. (2005). Comparison of fi-  
916 nite difference and boundary integral solutions to three-dimensional sponta-  
917 neous rupture. *Journal of Geophysical Research: Solid Earth*, 110(B12). doi:  
918 10.1029/2005JB003813
- 919 Di Toro, G., Han, R., Hirose, T., De Paola, N., Nielsen, S., Mizoguchi, K., ... Shi-  
920 mamoto, T. (2011, mar). Fault lubrication during earthquakes. *Nature*, 471,  
921 494.
- 922 Dieterich, J. H. (1979). Modeling of rock friction 1. experimental results and consti-  
923 tutive equations. *Journal of Geophysical Research*, 84(B5), 2161-2168.

- 924 Douilly, R., Aochi, H., Calais, E., & Freed, A. M. (2015). Three-dimensional dy-  
 925 namic rupture simulations across interacting faults: The Mw 7.0, 2010, Haiti  
 926 earthquake. *Journal of Geophysical Research: Solid Earth*, *120*(2), 1108-1128.  
 927 doi: 10.1002/2014JB011595
- 928 Duan, B., & Oglesby, D. D. (2006). Heterogeneous fault stresses from previous  
 929 earthquakes and the effect on dynamics of parallel strike-slip faults. *Journal of  
 930 Geophysical Research: Solid Earth*, *111*(B5). doi: 10.1029/2005JB004138
- 931 Dunham, E. M., Belanger, D., Cong, L., & Kozdon, J. E. (2011a). Earthquake  
 932 ruptures with strongly rate-weakening friction and off-fault plasticity, part2:  
 933 Planar faults. *Bulletin of the Seismological Society of America*, *101*(5), 2296-  
 934 2307. doi: 10.1785/0120100075
- 935 Dunham, E. M., Belanger, D., Cong, L., & Kozdon, J. E. (2011b). Earthquake  
 936 ruptures with strongly rate-weakening friction and off-fault plasticity, part 2:  
 937 Nonplanar faults. *The Bulletin of the Seismological Society of America*, *101*,  
 938 2308-2322. doi: 10.1785/0120100076
- 939 Dunham, E. M., & Rice, J. R. (2008). Earthquake slip between dissimilar poroe-  
 940 lastic materials. *Journal of Geophysical Research: Solid Earth*, *113*(B9). doi:  
 941 <https://doi.org/10.1029/2007JB005405>
- 942 Erickson, B. A., & Day, S. M. (2016). Bimaterial effects in an earthquake cycle  
 943 model using rate-and-state friction. *Journal of Geophysical Research: Solid  
 944 Earth*, *121*(4), 2480-2506. doi: 10.1002/2015JB012470
- 945 Erickson, B. A., & Dunham, E. M. (2014). An efficient numerical method for  
 946 earthquake cycles in heterogeneous media: Alternating subbasin and surface-  
 947 rupturing events on faults crossing a sedimentary basin. *Journal of Geophysical  
 948 Research: Solid Earth*, *119*(4), 3290-3316. doi: 10.1002/2013JB010614
- 949 Erickson, B. A., Dunham, E. M., & Khosravifar, A. (2017). A finite difference  
 950 method for off-fault plasticity throughout the earthquake cycle. *Journal of the  
 951 Mechanics and Physics of Solids*, *109*, 50 - 77. doi: <https://doi.org/10.1016/>

- 952 j.jmps.2017.08.002
- 953 Erickson, B. A., Jiang, J., Barall, M., Lapusta, N., Dunham, E. M., Harris, R., ...
- 954 Wei, M. (2020). The Community Code Verification Exercise for Simulating  
955 Sequences of Earthquakes and Aseismic Slip (SEAS). *Seismological Research  
Letters*, 91(2A), 874–890. doi: 10.1785/0220190248
- 956 Field, E. H. (2019). How Physics Based Earthquake Simulators Might Help Improve  
957 Earthquake Forecasts. *Seismological Research Letters*, 90(2A), 467-472. doi: 10  
958 .1785/0220180299
- 959 Field, E. H., Biasi, G., Bird, P., Dawson, T., Felzer, K.R., ... Zeng, Y. (2013).  
960 Uniform California Earthquake Rupture Forecast, version 3 (UCERF3)  
961 –the time-independent model. *U.S. Geological Survey Open-File Report  
962 2013-1165*, 97 p., *California Geological Survey Special Report 228*. doi:  
963 <http://pubs.usgs.gov/of/2013/1165/>
- 964 Field, E. H., Jordan, T. H., Page, M. T., Milner, K. R., Shaw, B. E., Dawson, T. E.,  
965 ... Thatcher, W. R. (2017). A synoptic view of the third Uniform California  
966 Earthquake Rupture Forecast (UCERF3). *Seismological Research Letters*,  
967 88(5), 1259-1267. doi: 10.1785/0220170045
- 968 Fulton, P. M., Brodsky, E. E., Kano, Y., Mori, J., Chester, F., Ishikawa, T., ...  
969 Scientists, K.-. (2013). Low coseismic friction on the Tohoku-Oki fault deter-  
970 mined from temperature measurements. *Science*, 342(6163), 1214–1217. doi:  
971 10.1126/science.1243641
- 972 Galvez, P., Ampuero, J.-P., Dalguer, L. A., Somalia, S. N., & Nissen-Meyer, T.  
973 (2014). Dynamic earthquake rupture modelled with an unstructured 3-D spec-  
974 tral element method applied to the 2011 M9 Tohoku earthquake. *Geophysical  
975 Journal International*, 198(2), 1222-1240. doi: 10.1093/gji/ggu203
- 976 Harris, R., Archuleta, R. J., & Day, S. M. (1991). Fault steps and the dynamic  
977 rupture process: 2-D numerical simulations of a spontaneously propagat-  
978 ing shear fracture. *Geophysical Research Letters*, 18(5), 893-896. doi:  
979

- 980 10.1029/91GL01061
- 981 Harris, R., Barall, M., Aagaard, B., Ma, S., Roten, D., Olsen, K., ... Dalguer, L.
- 982 (2018). A Suite of Exercises for Verifying Dynamic Earthquake Rupture Codes.
- 983 *Seismological Research Letters*, 89(3), 1146-1162. doi: 10.1785/0220170222
- 984 Harris, R., Barall, M., Archuleta, R., Dunham, E., Aagaard, B., Ampuero, J. P.,
- 985 ... Templeton, E. (2009). The SCEC/USGS dynamic earthquake rup-
- 986 ture code verification exercise. *Seismological Research Letters*, 80. doi:
- 987 10.1785/gssrl.80.1.119
- 988 Harris, R., & Day, S. M. (1993). Dynamics of fault interaction: parallel strike-slip
- 989 faults. *Journal of Geophysical Research: Solid Earth*, 98(B3), 4461-4472. doi:
- 990 10.1029/92JB02272
- 991 Harris, R., & Day, S. M. (1999). Dynamic 3D simulations of earthquakes on en
- 992 echelon faults. *Geophysical Research Letters*, 26(14), 2089-2092. doi: 10.1029/
- 993 1999GL900377
- 994 Hauksson, E., Yang, W., & Shearer, P. M. (2012). Waveform Relocated Earthquake
- 995 Catalog for Southern California (1981 to June 2011). *Bulletin of the Seismological*
- 996 *Society of America*, 102(5), 2239-2244. doi: 10.1785/0120120010
- 997 Henyey, T. L., & Wasserburg, G. J. (1971). Heat flow near major strike-slip faults
- 998 in California. *Journal of Geophysical Research (1896-1977)*, 76(32), 7924-7946.
- 999 doi: 10.1029/JB076i032p07924
- 1000 Hillers, G., Ben-Zion, Y., & Mai, P. M. (2006). Seismicity on a fault controlled
- 1001 by rate- and state-dependent friction with spatial variations of the crit-
- 1002 ical slip distance. *Journal of Geophysical Research*, 111, B01403. doi:
- 1003 10.1029/2005JB003859
- 1004 Hillers, G., Mai, P. M., Ben-Zion, Y., & Ampuero, J.-P. (2007). Statistical prop-
- 1005 erties of seismicity of fault zones at different evolutionary stages. *Geophysical*
- 1006 *Journal International*, 169(2), 515-533. doi: 10.1111/j.1365-246X.2006.03275
- 1007 .X

- 1008 Hu, F., Zhang, Z., & Chen, X. (2016). Investigation of earthquake jump distance for  
1009 strike-slip step overs based on 3-D dynamic rupture simulations in an elastic  
1010 half-space. *Journal of Geophysical Research: Solid Earth*, *121*(2), 994-1006.  
1011 doi: [10.1002/2015JB012696](https://doi.org/10.1002/2015JB012696)
- 1012 Huang, J., & Turcotte, D. L. (1990). Are earthquakes an example of deterministic  
1013 chaos? *Geophysical Research Letters*, *17*(3), 223-226. doi: <https://doi.org/10.1029/GL017i003p00223>
- 1014 Ishibe, T., & Shimazaki, K. (2012). Characteristic Earthquake Model and Seismicity  
1015 around Late Quaternary Archive Faults in Japan. *Bulletin of the Seismological  
1016 Society of America*, *102*(3), 1041-1058. doi: [10.1785/0120100250](https://doi.org/10.1785/0120100250)
- 1017 Ito, Y., Hino, R., Kido, M., Fujimoto, H., Osada, Y., Inazu, D., ... Ashi, J.  
1018 (2013). Episodic slow slip events in the Japan subduction zone before  
1019 the 2011 Tohoku-Oki earthquake. *Tectonophysics*, *600*, 14-26. doi:  
1020 <https://doi.org/10.1016/j.tecto.2012.08.022>
- 1021 Jiang, J., & Lapusta, N. (2016). Deeper penetration of large earthquakes on seis-  
1022 mically quiescent faults. *Science*, *352*(6291), 1293–1297. doi: [10.1126/science.aaf1496](https://doi.org/10.1126/science.aaf1496)
- 1023 Johnson, E. (1992). The influence of the lithospheric thickness on bilateral slip.  
1024 *Geophysical Journal International*, *108*(1), 151-160. doi: [10.1111/j.1365-246X.1992.tb00846.x](https://doi.org/10.1111/j.1365-246X.1992.tb00846.x)
- 1025 Kagan, Y. Y., Jackson, D. D., & Geller, R. J. (2012). Characteristic Earthquake  
1026 Model, 1884–2011, RIP. *Seismological Research Letters*, *83*(6), 951-953. doi:  
1027 [10.1785/0220120107](https://doi.org/10.1785/0220120107)
- 1028 Kame, N., Rice, J. R., & Dmowska, R. (2003). Effects of prestress state and rupture  
1029 velocity on dynamic fault branching. *Journal of Geophysical Research: Solid  
1030 Earth*, *108*(B5). doi: [10.1029/2002JB002189](https://doi.org/10.1029/2002JB002189)
- 1031 Kaneko, Y., Avouac, J.-P., & Lapusta, N. (2010). Towards inferring earthquake pat-  
1032 terns from geodetic observations of interseismic coupling. *Nature Geoscience*,  
1033  
1034

- 1036                   3, 363–369. doi: 10.1038/NGEO843
- 1037                   Kaneko, Y., & Lapusta, N. (2008). Variability of earthquake nucleation in con-  
tinuum models of rate-and-state faults and implications for aftershock rates.  
*Journal of Geophysical Research*, 113, B12312. doi: 10.1029/2007JB005154
- 1039  
1040                   Kato, A., Obara, K., Igarashi, T., Tsuruoka, H., Nakagawa, S., & Hirata, N. (2012).  
Propagation of slow slip leading up to the 2011 Mw 9.0 Tohoku-Oki earth-  
quake. *Science*, 335(6069), 705–708. doi: 10.1126/science.1215141
- 1041  
1042                   Kato, N. (2014, 06). Deterministic chaos in a simulated sequence of slip events on  
a single isolated asperity. *Geophysical Journal International*, 198(2), 727–736.  
doi: 10.1093/gji/ggu157
- 1043  
1044                   Lachenbruch, A. H., & Sass, J. H. (1980). Heat flow and energetics of the san an-  
dreas fault zone. *Journal of Geophysical Research: Solid Earth*, 85(B11), 6185–  
6222. doi: 10.1029/JB085iB11p06185
- 1045  
1046                   Lambert, V., & Barbot, S. (2016). Contribution of viscoelastic flow in earthquake  
cycles within the lithosphere-asthenosphere system. *Geophysical Research Letters*,  
43(19), 10,142–10,154. doi: 10.1002/2016GL070345
- 1047  
1048                   Lambert, V., & Lapusta, N. (2020). Rupture-dependent breakdown energy in fault  
models with thermo-hydro-mechanical processes. *Solid Earth*, 11(6), 2283–  
2302. doi: 10.5194/se-11-2283-2020
- 1049  
1050                   Lambert, V., Lapusta, N., & Faulkner, D. (in review). Scale dependence of earth-  
quake rupture prestress in models with enhanced weakening: implications for  
event statistics and inferences of fault stress. *Journal of Geophysical Research:*  
*Solid Earth*, 55. doi: 10.1002/essoar.10506240.1
- 1051  
1052                   Lambert, V., Lapusta, N., & Perry, S. (2021). Propagation of large earthquakes as  
self-healing pulses or mild cracks. *Nature*, 591(7849), 252–258. doi: 10.1038/  
s41586-021-03248-1
- 1053  
1054                   Lapusta, N., & Liu, Y. (2009). Three-dimensional boundary integral modeling of  
spontaneous earthquake sequences and aseismic slip. *Journal of Geophysical*

1064 *Research*, 114, B09303. doi: 10.1029/2008JB005934

1065 Lapusta, N., & Rice, J. (2003). Low-heat and low-stress fault operation in earth-  
1066 quake models of statically strong but dynamically weak faults. *AGU Fall*  
1067 *Meeting Abstracts.*

Lapusta, N., Rice, J. R., Ben-Zion, Y., & Zheng, G. (2000). Elastodynamic analysis  
for slow tectonic loading with spontaneous rupture episodes on faults with  
rate- and state- dependent friction. *Journal of Geophysical Research, 105*,

Lehner, F. K., Li, V. C., & Rice, J. R. (1981). Stress diffusion along rupturing plate  
boundaries. *Journal of Geophysical Research: Solid Earth*, 86(B7), 6155-6169.  
doi: 10.1029/JB086iB07p06155

1075 Lin, Y.-Y., & Lapusta, N. (2018). Microseismicity simulated on asperity-like fault  
1076 patches: On scaling of seismic moment with duration and seismological esti-  
1077 mates of stress drops. *Geophysical Research Letters*, 45(16), 8145-8155. doi:  
1078 10.1029/2018GL078650

Liu, Y. (2014). Source scaling relations and along-strike segmentation of slow slip events in a 3-D subduction fault model. *Journal of Geophysical Research: Solid Earth*, 119(8), 6512-6533. doi: 10.1002/2014JB011144

Liu, Y., & Rice, J. R. (2005). Aseismic slip transients emerge spontaneously in three-dimensional rate and state modeling of subduction earthquake sequences. *Journal of Geophysical Research: Solid Earth*, 110(B8). doi: 10.1029/2004JB003424

Liu, Y., & Rice, J. R. (2007). Spontaneous and triggered aseismic deformation transients in a subduction fault model. *Journal of Geophysical Research: Solid Earth*, 112(B9). doi: 10.1029/2007JB004930

1089 Lozos, J. C., Oglesby, D. D., Brune, J. N., & Olsen, K. B. (2015). Rupture and  
1090 Ground-Motion Models on the Northern San Jacinto Fault, Incorporating Re-  
1091 alistic Complexity. *Bulletin of the Seismological Society of America*, 105(4),

- 1092 1931-1946. doi: 10.1785/0120140327
- 1093 Lyakhovsky, V., & Ben-Zion, Y. (2009). Evolving geometrical and material prop-  
1094 erties of fault zones in a damage rheology model. *Geochemistry, Geophysics,  
1095 Geosystems*, 10(11). doi: <https://doi.org/10.1029/2009GC002543>
- 1096 Lyakhovsky, V., & Ben-Zion, Y. (2014). Damage breakage rheology model  
1097 and solid-granular transition near brittle instability. *Journal of the Me-  
1098 chanics and Physics of Solids*, 64, 184-197. doi: <https://doi.org/10.1016/j.jmps.2013.11.007>
- 1099 Mele Veedu, D., & Barbot, S. (2016). The parkfield tremors reveal slow and  
1100 fast ruptures on the same asperity. *Nature*, 532, 361-365. doi: 10.1038/nature17190
- 1101 Michailos, K., Smith, E. G., Chamberlain, C. J., Savage, M. K., & Townend, J.  
1102 (2019). Variations in seismogenic thickness along the Central Alpine Fault,  
1103 New Zealand, revealed by a decade's relocated microseismicity. *Geochemistry,  
1104 Geophysics, Geosystems*, 20(1), 470-486. doi: 10.1029/2018GC007743
- 1105 Michel, S., Avouac, J.-P., Lapusta, N., & Jiang, J. (2017). Pulse-like partial ruptures  
1106 and high-frequency radiation at creeping-locked transition during megath-  
1107 rust earthquakes. *Geophysical Research Letters*, 44(16), 8345-8351. doi:  
1108 10.1002/2017GL074725
- 1109 Noda, H., & Lapusta, N. (2010). Three-dimensional earthquake sequence simulations  
1110 with evolving temperature and pore pressure due to shear heating: Effect of  
1111 heterogeneous hydraulic diffusivity. *Journal of Geophysical Research*, 115,  
1112 B123414. doi: 10.1029/2010JB007780
- 1113 Noda, H., & Lapusta, N. (2013). Stable creeping fault segments can become destruc-  
1114 tive as a result of dynamic weakening. *Nature*, 493, 518 EP -.
- 1115 Noda, H., Lapusta, N., & Kanamori, H. (2013). Comparison of average stress  
1116 drop measures for ruptures with heterogeneous stress change and impli-  
1117 cations for earthquake physics. *Geophysical Journal International*. doi:  
1118

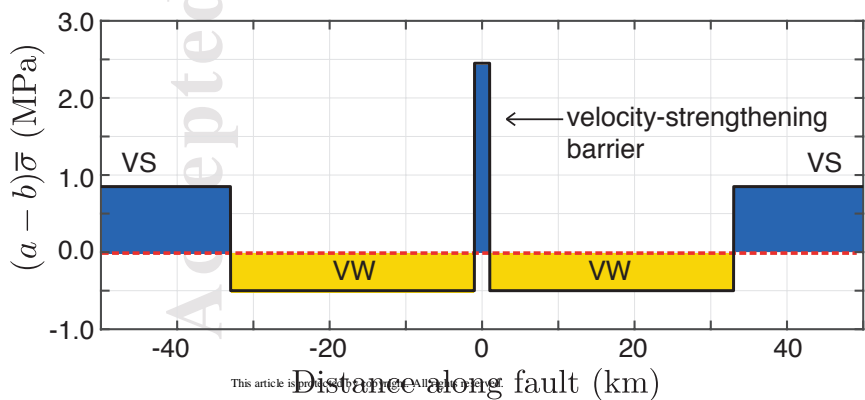
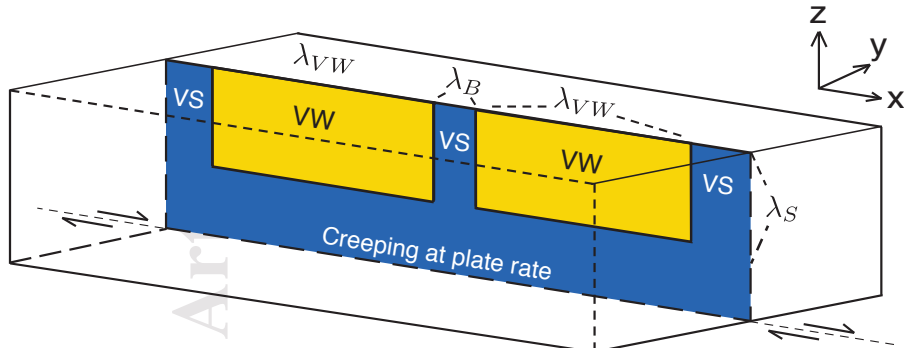
- 1120 10.1093/gji/ggt074
- 1121 Okubo, K., Bhat, H. S., Rougier, E., Marty, S., Schubnel, A., Lei, Z., ... Klinger, Y.  
 1122 (2019). Dynamics, radiation, and overall energy budget of earthquake rupture  
 1123 with coseismic off-fault damage. *Journal of Geophysical Research: Solid Earth*,  
 1124 124(11), 11771-11801. doi: 10.1029/2019JB017304
- 1125 Olami, Z., Feder, H. J. S., & Christensen, K. (1992). Self-organized criticality in  
 1126 a continuous, nonconservative cellular automaton modeling earthquakes. *Phys.  
 1127 Rev. Lett.*, 68, 1244–1247. doi: 10.1103/PhysRevLett.68.1244
- 1128 Page, M. T., & Felzer, K. (2015). Southern San Andreas Fault seismicity is  
 1129 consistent with the Gutenberg-Richter magnitude-frequency distribution.  
 1130 *Bulletin of the Seismological Society of America*, 105(4), 2070-2080. doi:  
 1131 10.1785/0120140340
- 1132 Page, M. T., & van der Elst, N. J. (2018). Fault-tolerant b-values and aftershock  
 1133 productivity. *Journal of Geophysical Research: Solid Earth*, 123(12), 10,880-  
 1134 10,888. doi: <https://doi.org/10.1029/2018JB016445>
- 1135 Parsons, T. (2008). Monte carlo method for determining earthquake recur-  
 1136 rence parameters from short paleoseismic catalogs: Example calculations  
 1137 for california. *Journal of Geophysical Research: Solid Earth*, 113(B3). doi:  
 1138 <https://doi.org/10.1029/2007JB004998>
- 1139 Perrin, G., Rice, J. R., & Zheng, G. (1995). Self-healing slip pulse on a frictional  
 1140 surface. *Journal of the Mechanics and Physics of Solids*, 43(9), 1461 - 1495.  
 1141 doi: [https://doi.org/10.1016/0022-5096\(95\)00036-I](https://doi.org/10.1016/0022-5096(95)00036-I)
- 1142 Perry, S. M., Lambert, V., & Lapusta, N. (2020). Nearly magnitude-invariant stress  
 1143 drops in simulated crack-like earthquake sequences on rate-and-state faults  
 1144 with thermal pressurization of pore fluids. *Journal of Geophysical Research:  
 1145 Solid Earth*, 125(3), e2019JB018597. doi: 10.1029/2019JB018597
- 1146 Poliakov, A. N. B., Dmowska, R., & Rice, J. R. (2002). Dynamic shear rup-  
 1147 ture interactions with fault bends and off-axis secondary faulting. *Journal*

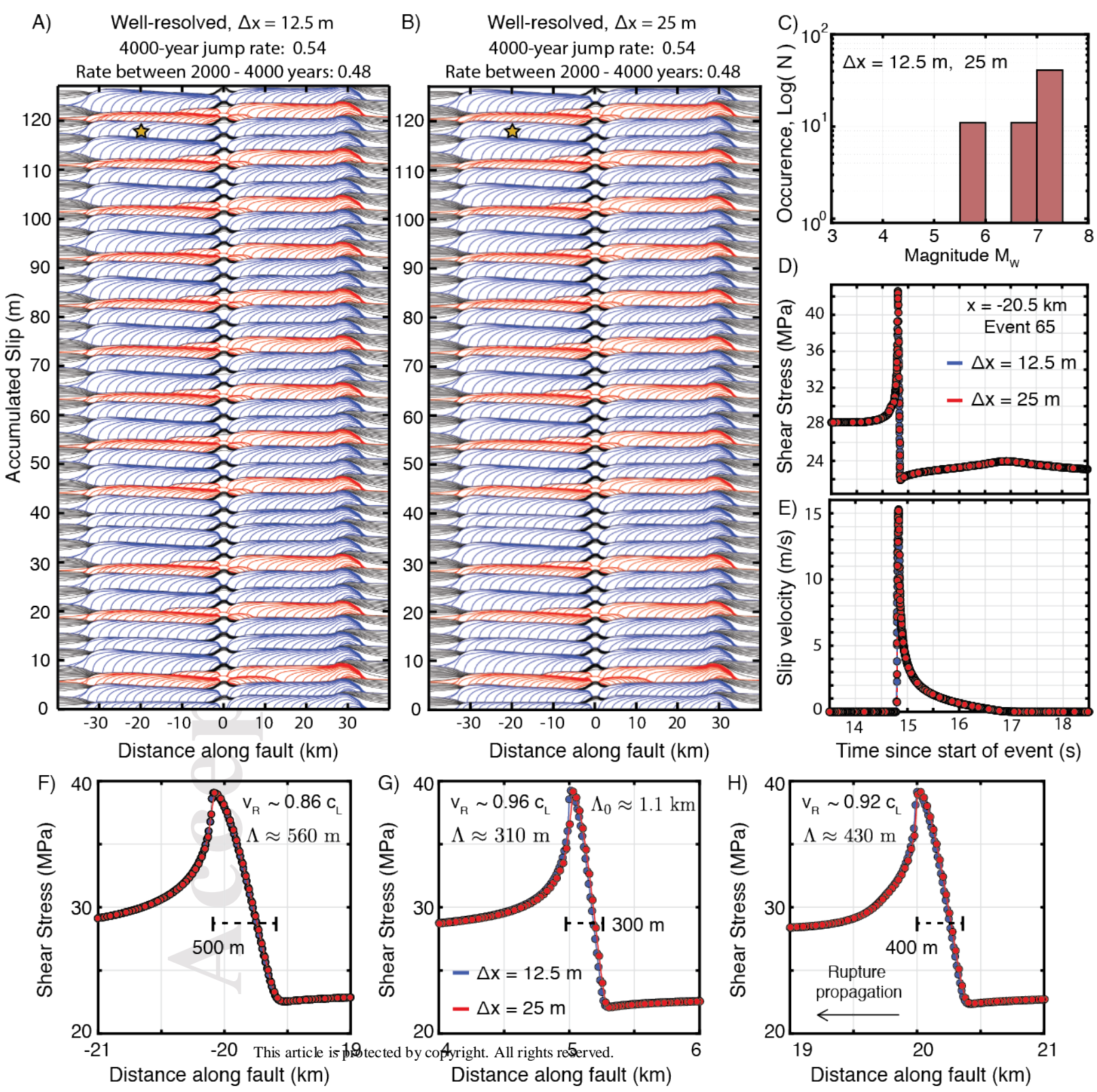
- 1148                   of *Geophysical Research: Solid Earth*, 107(B11), ESE 6-1-ESE 6-18. doi:  
 1149                   10.1029/2001JB000572
- 1150                   Rice, J. R. (1980). The mechanics of earthquake rupture. in *Physics of Earth's*  
 1151                   *Interior*, 555-649.
- 1152                   Rice, J. R. (1993). Spatio-temporal complexity of slip on a fault. *Journal of Geo-*  
 1153                   *physical Research: Solid Earth*, 98(B6), 9885-9907. doi: 10.1029/93JB00191
- 1154                   Rice, J. R. (2006). Heating and weakening of faults during earthquake slip. *Journal*  
 1155                   *of Geophysical Research*, 111, B05311. doi: 10.1029/2005JB004006
- 1156                   Rice, J. R., & Ben-Zion, Y. (1996, 04). Slip complexity in earthquake fault mod-  
 1157                   els. *Proceedings of the National Academy of Sciences of the United States of*  
 1158                   *America*, 93(9), 3811–3818. doi: 10.1073/pnas.93.9.3811
- 1159                   Rice, J. R., & Ruina, A. L. (1983). Stability of steady frictional slipping. *Journal of*  
 1160                   *Applied Mechanics*, 50(2), 343-349.
- 1161                   Richards-Dinger, K., & Dieterich, J. H. (2012). RSQSim Earthquake Simulator.  
 1162                   *Seismological Research Letters*, 83(6), 983-990. doi: 10.1785/0220120105
- 1163                   Ross, Z. E., Cochran, E. S., Trugman, D. T., & Smith, J. D. (2020). 3d fault ar-  
 1164                   chitecture controls the dynamism of earthquake swarms. *Science*, 368(6497),  
 1165                   1357–1361. doi: 10.1126/science.abb0779
- 1166                   Ross, Z. E., Trugman, D. T., Hauksson, E., & Shearer, P. M. (2019). Searching for  
 1167                   hidden earthquakes in southern California. *Science*, 364(6442), 767–771. doi:  
 1168                   10.1126/science.aaw6888
- 1169                   Rubin, A., & Ampuero, J.-P. (2005). Earthquake nucleation on (aging) rate and  
 1170                   state faults. *Journal of Geophysical Research: Solid Earth*, 110(B11).
- 1171                   Rudnicki, J., & Rice, J. (1975). Conditions for the localization of deformation in  
 1172                   pressure-sensitive dilatant materials. *Journal of the Mechanics and Physics of*  
 1173                   *Solids*, 23(6), 371-394. doi: [https://doi.org/10.1016/0022-5096\(75\)90001-0](https://doi.org/10.1016/0022-5096(75)90001-0)
- 1174                   Ruina, A. (1983). Slip instability and state variable friction laws. *Journal of*  
 1175                   *Geophysical Research*, 88(B12), 10359-10370.

- 1176 Ruiz, S., Metois, M., Fuenzalida, A., Ruiz, J., Leyton, F., Grandin, R., ... Cam-  
 1177 pos, J. (2014). Intense foreshocks and a slow slip event preceded the  
 1178 2014 Iquique Mw 8.1 earthquake. *Science*, *345*(6201), 1165–1169. doi:  
 1179 [10.1126/science.1256074](https://doi.org/10.1126/science.1256074)
- 1180 Schorlemmer, D., & Wiemer, S. (2005). Microseismicity data forecast rupture area.  
 1181 *Nature*, *434*(7037), 1086–1086. doi: [10.1038/4341086a](https://doi.org/10.1038/4341086a)
- 1182 Schwartz, D. P., & Coppersmith, K. J. (1984). Fault behavior and characteristic  
 1183 earthquakes—examples from the wasatch and san andreas fault zones. *Journal*  
 1184 *of Geophysical Research*, *89*, 5681–5698.
- 1185 Segall, P., & Rice, J. R. (1995). Dilatancy, compaction, and slip instability of a  
 1186 fluid-infiltrated fault. *Journal of Geophysical Research: Solid Earth*, *100*(B11),  
 1187 22155–22171. doi: [10.1029/95JB02403](https://doi.org/10.1029/95JB02403)
- 1188 Segall, P., Rubin, A. M., Bradley, A. M., & Rice, J. R. (2010). Dilatant strengthen-  
 1189 ing as a mechanism for slow slip events. *Journal of Geophysical Research: Solid*  
 1190 *Earth*, *115*(B12). doi: [10.1029/2010JB007449](https://doi.org/10.1029/2010JB007449)
- 1191 Shaw, B. E., Milner, K. R., Field, E. H., Richards-Dinger, K., Gilchrist, J. J., Di-  
 1192 eterich, J. H., & Jordan, T. H. (2018). A physics-based earthquake simulator  
 1193 replicates seismic hazard statistics across california. *Science Advances*, *4*(8).  
 1194 doi: [10.1126/sciadv.aau0688](https://doi.org/10.1126/sciadv.aau0688)
- 1195 Sieh, K. E. (1978). Central California foreshocks of the great 1857 earthquake.  
 1196 *Bulletin of the Seismological Society of America*, *68*(6), 1731–1749.
- 1197 Sieh, K. E., Jones, L., Hauksson, E., Hudnut, K., Eberhart-Phillips, D., Heaton,  
 1198 T., ... Zachariasen, J. (1993). Near-field investigations of the Landers  
 1199 Earthquake Sequence, April to July 1992. *Science*, *260*(5105), 171–176. doi:  
 1200 [10.1126/science.260.5105.171](https://doi.org/10.1126/science.260.5105.171)
- 1201 Stirling, M. W., Wesnousky, S. G., & Shimazaki, K. (1996). Fault trace complexity,  
 1202 cumulative slip, and the shape of the magnitude-frequency distribution for  
 1203 strike-slip faults: a global survey. *Geophysical Journal International*, *124*(3),

- 1204 833-868. doi: 10.1111/j.1365-246X.1996.tb05641.x
- 1205 Thomas, M. Y., Lapusta, N., Noda, H., & Avouac, J.-P. (2014). Quasi-dynamic  
1206 versus fully dynamic simulations of earthquakes and aseismic slip with and  
1207 without enhanced coseismic weakening. *Journal of Geophysical Research*, 119,  
1208 1986-2004. doi: 10.1002/2013JB010615
- 1209 Tullis, T. (2007). Friction of rock at earthquake slip rates. *Treatise on Geophysics*,  
1210 4, 131-152. doi: 10.1016/B978-044452748-6.00064-X
- 1211 Tullis, T., Richards-Dinger, K., Barall, M., Dieterich, J. H., Field, E. H., Heien,  
1212 E. M., ... Yikilmaz, M. B. (2012). Generic Earthquake Simulator. *Seismological  
1213 Research Letters*, 83(6), 959-963. doi: 10.1785/0220120093
- 1214 Ulrich, T., Gabriel, A.-A., Ampuero, J.-P., & Xu, W. (2019). Dynamic viability of  
1215 the 2016 Mw 7.8 Kaikoura earthquake cascade on weak crustal faults. *Nature  
1216 Communications*, 10(1), 1213. doi: 10.1038/s41467-019-09125-w
- 1217 Viesca, R. C., & Garagash, D. I. (2015). Ubiquitous weakening of faults due to ther-  
1218 mal pressurization. *Nature Geoscience*, 8, 875-879. doi: 10.1038/NGEO2554
- 1219 Wei, S., Helmberger, D., & Avouac, J.-P. (2013). Modeling the 2012 Wharton basin  
1220 earthquakes off-Sumatra: Complete lithospheric failure. *Journal of Geophysical  
1221 Research: Solid Earth*, 118(7), 3592-3609. doi: 10.1002/jgrb.50267
- 1222 Wesnousky, S. G. (1994). The Gutenberg-Richter or characteristic earthquake dis-  
1223 tribution, which is it? *Bulletin of the Seismological Society of America*, 84(6),  
1224 1940-1959.
- 1225 Withers, K. B., Olsen, K. B., Day, S. M., & Shi, Z. (2018). Ground Motion and In-  
1226 traevent Variability from 3D Deterministic Broadband (0-7.5 Hz) Simulations  
1227 along a Nonplanar Strike-Slip Fault. *Bulletin of the Seismological Society of  
1228 America*, 109(1), 229-250. doi: 10.1785/0120180006
- 1229 Wollherr, S., Gabriel, A.-A., & Mai, P. M. (2019). Landers 1992 reloaded: Integra-  
1230 tive dynamic earthquake rupture modeling. *Journal of Geophysical Research:  
1231 Solid Earth*, 124(7), 6666-6702. doi: 10.1029/2018JB016355

- 1232 Wu, Y., & Chen, X. (2014). The scale-dependent slip pattern for a uniform fault  
1233 model obeying the rate- and state-dependent friction law. *Journal of Geophysical Research: Solid Earth*, 119(6), 4890-4906. doi: 10.1002/2013JB010779
- 1234 Ye, L., Lay, T., Kanamori, H., & Rivera, L. (2016). Rupture characteristics of major  
1235 and great ( $M_w > 7.0$ ) megathrust earthquakes from 1990 to 2015: 2. depth  
1236 dependence. *Journal of Geophysical Research: Solid Earth*, 121(2), 845-863.  
1237 doi: 10.1002/2015JB012427
- 1238 Zhu, W., Allison, K. L., Dunham, E. M., & Yang, Y. (2020). Fault valving and  
1239 pore pressure evolution in simulations of earthquake sequences and aseismic  
1240 slip. *Nature Communications*, 11(1), 4833. Retrieved from <https://doi.org/10.1038/s41467-020-18598-z> doi: 10.1038/s41467-020-18598-z  
1241  
1242



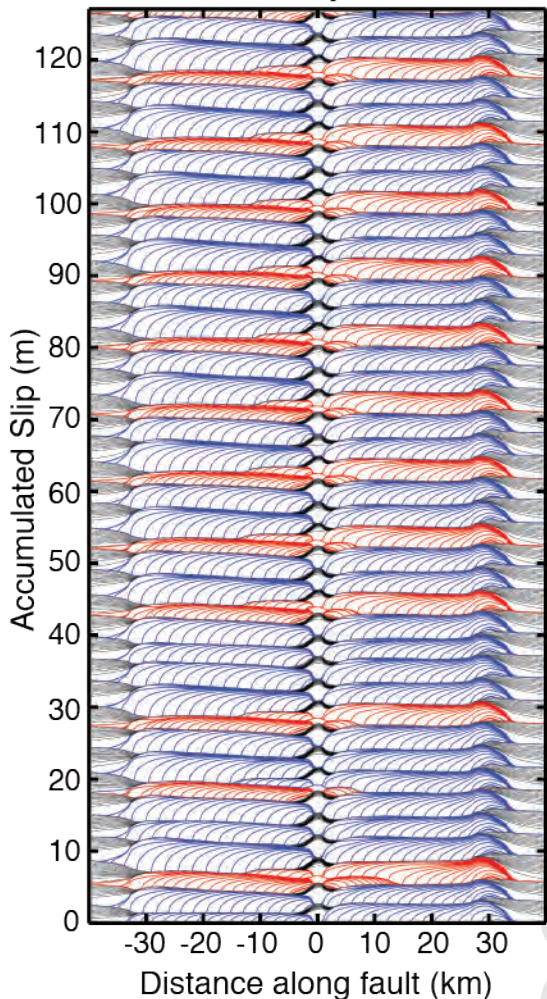


A)

Initial shear stress conditions S1  
Adequately discretized,  $\Delta x = 12.5$  m  
Jump rate between:

0 - 4000 years: 0.54  
2000 - 4000 years: 0.48

0 - 20,000 years: 0.51  
2000 - 20,000 years: 0.50

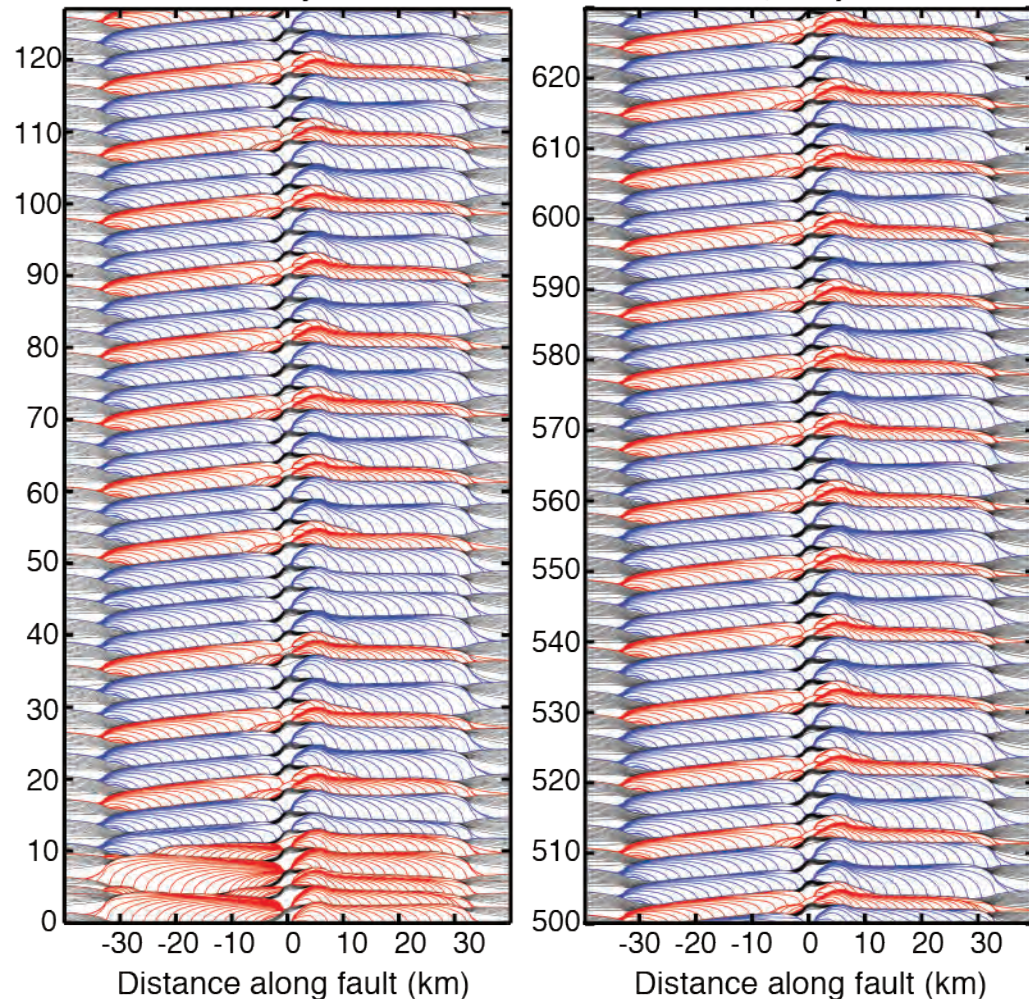


B)

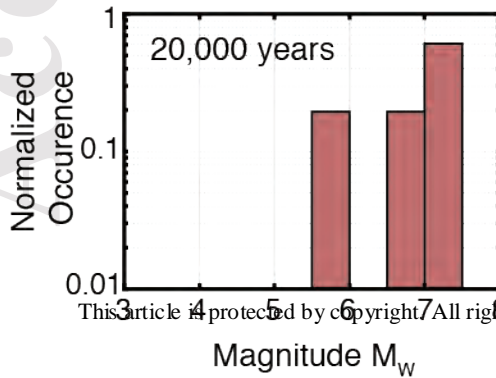
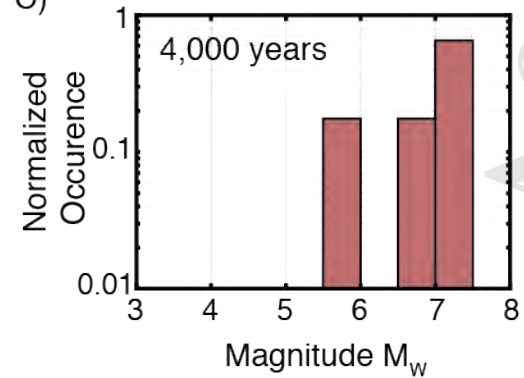
Initial shear stress conditions S2  
Adequately discretized,  $\Delta x = 12.5$  m  
Jump rate between:

0 - 4000 years: 0.48  
2000 - 4000 years: 0.52

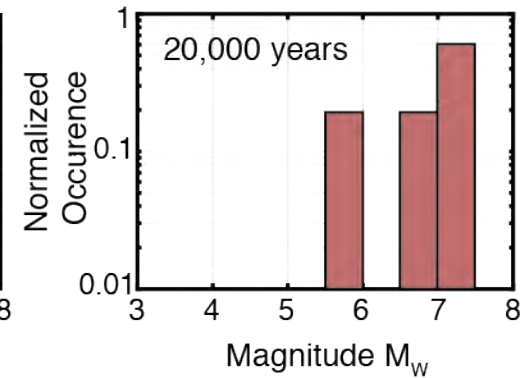
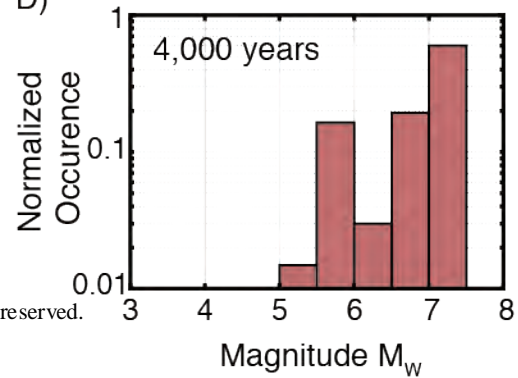
0 - 20,000 years: 0.50  
2000 - 20,000 years: 0.50

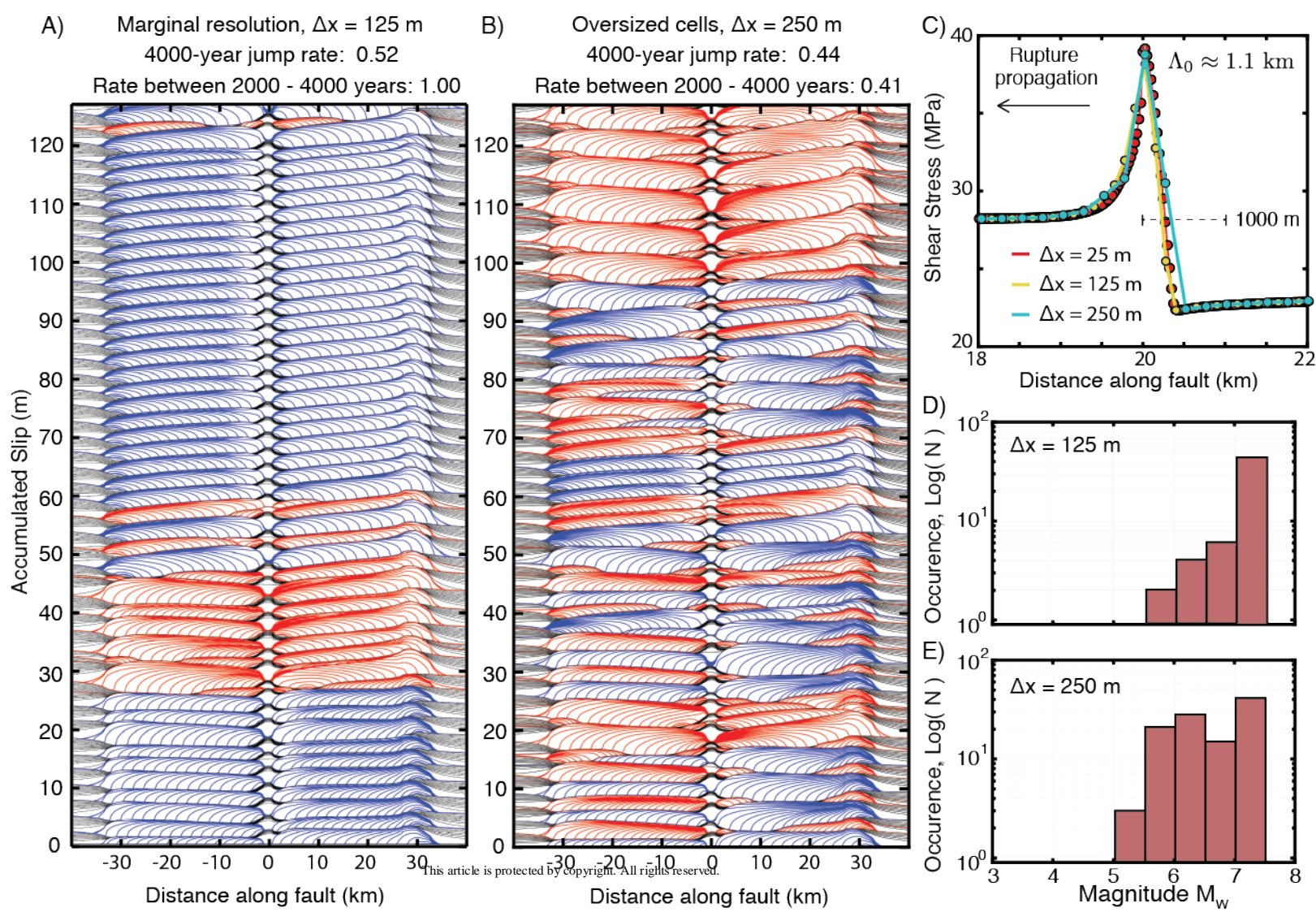


C)

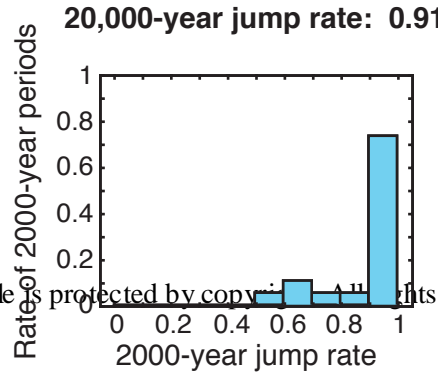
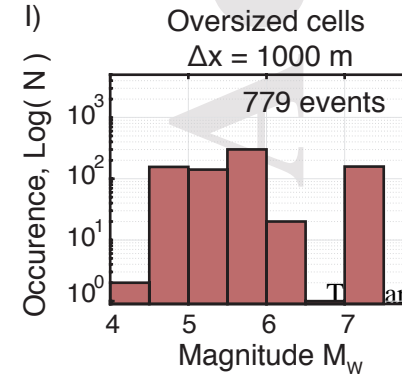
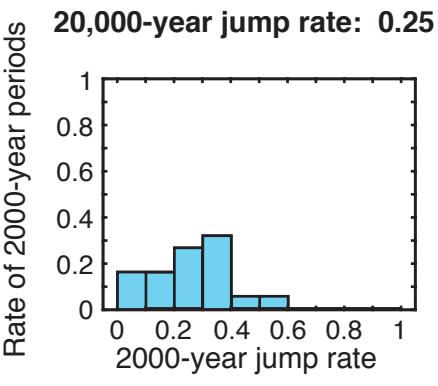
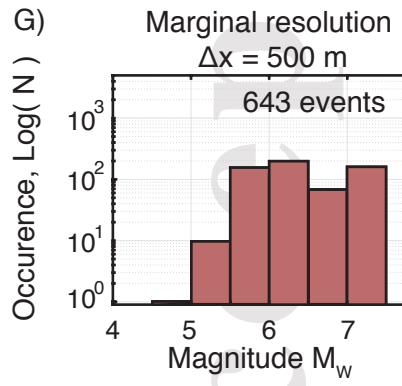
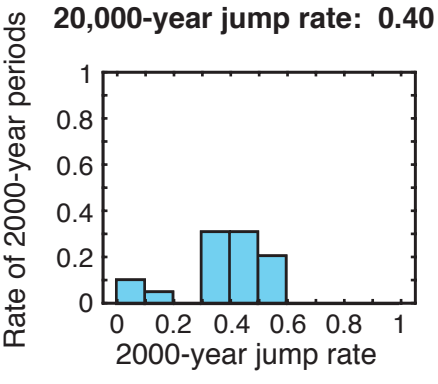
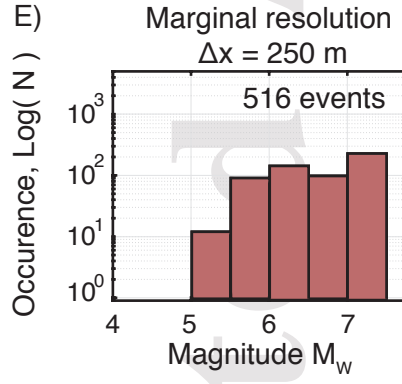
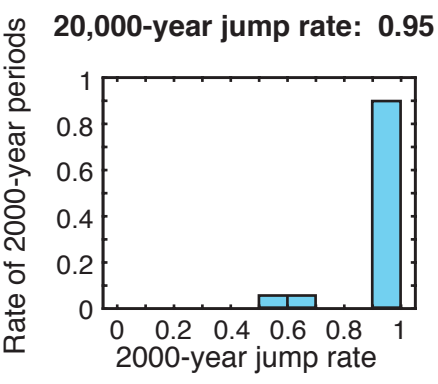
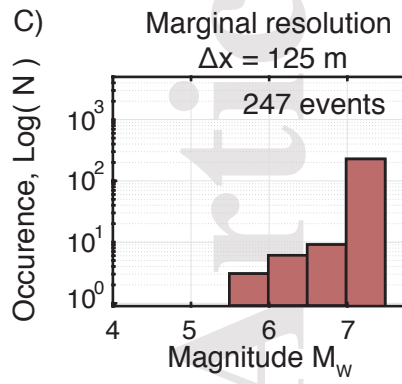
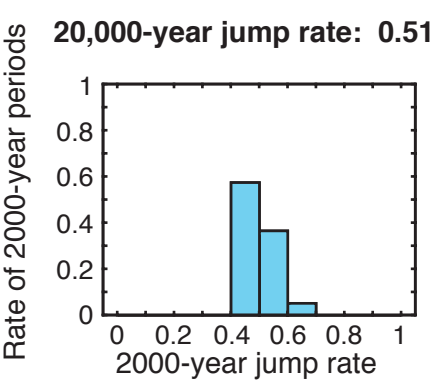
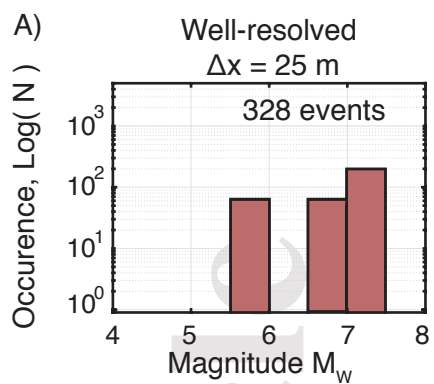


D)

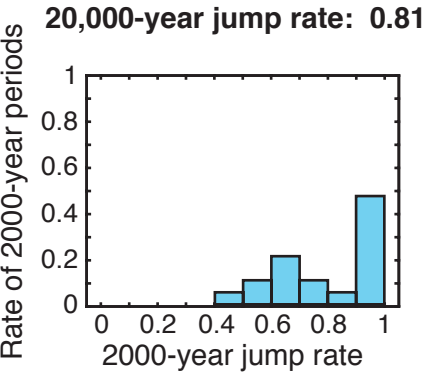
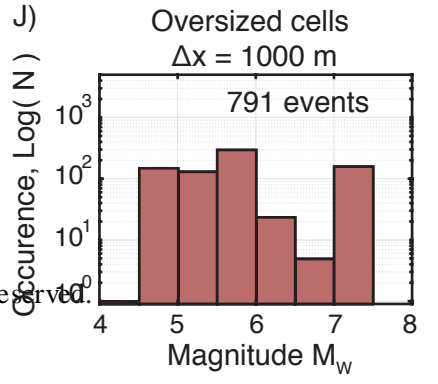
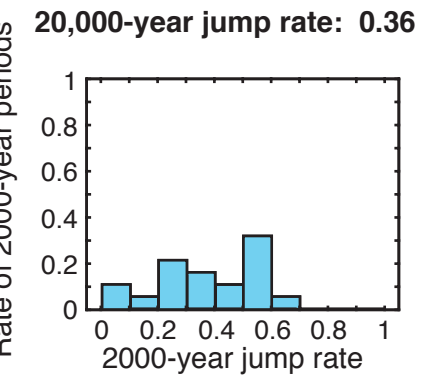
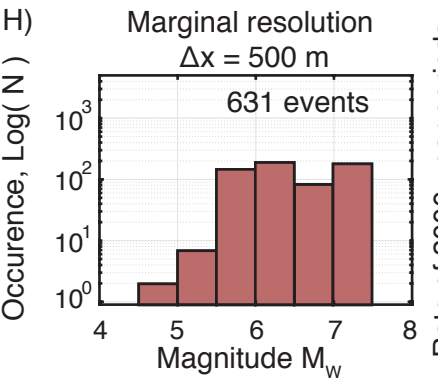
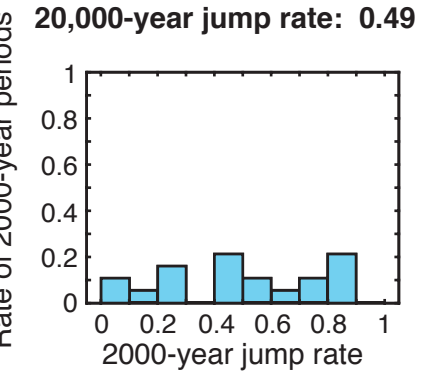
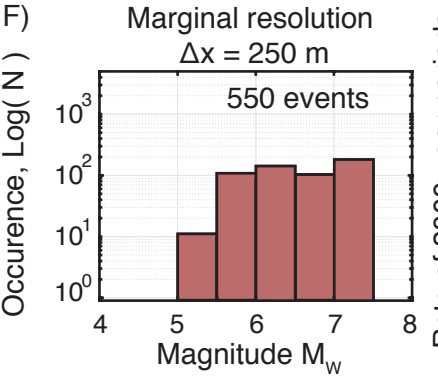
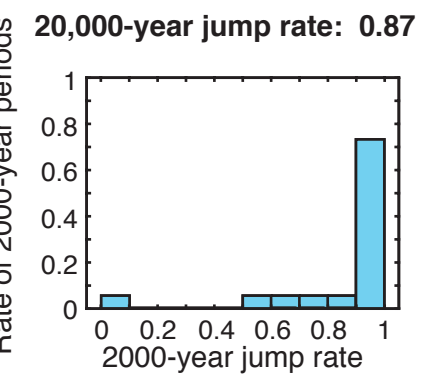
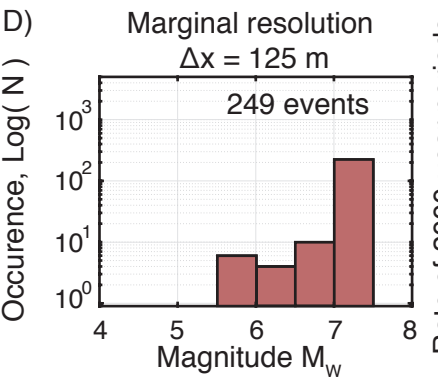
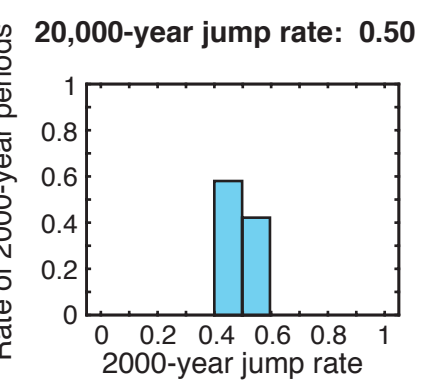
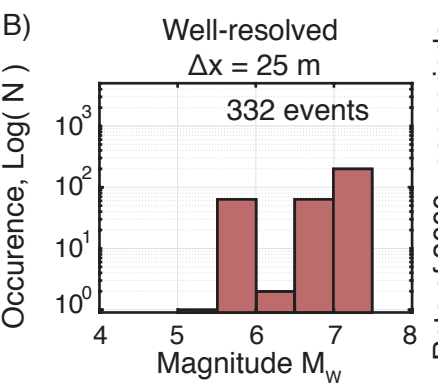




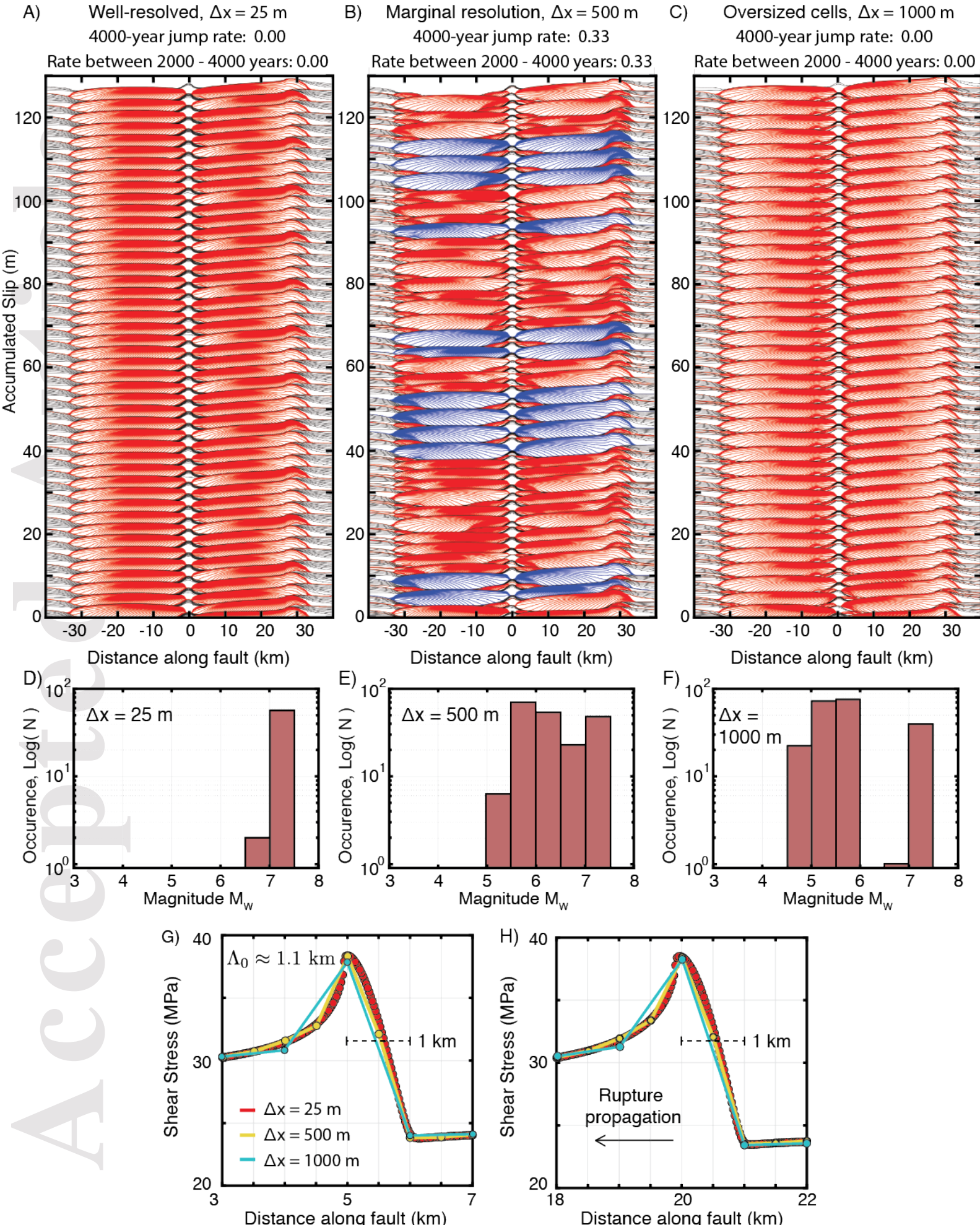
### Initial shear stress conditions S1

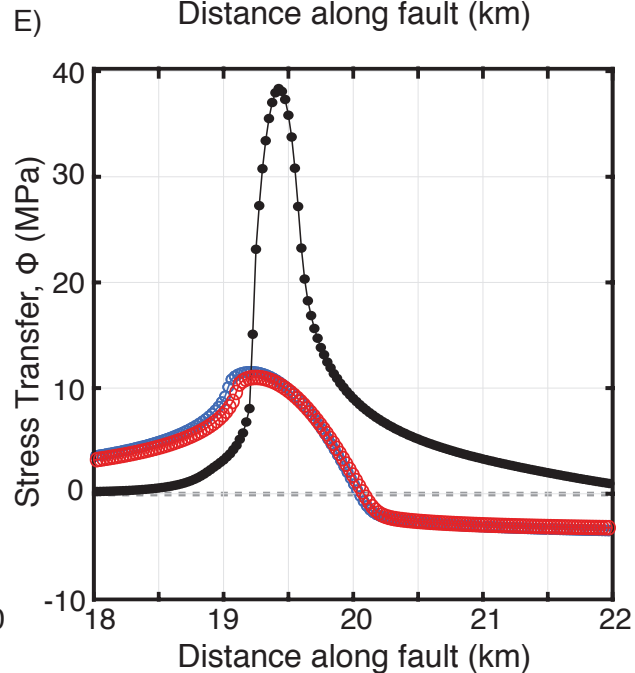
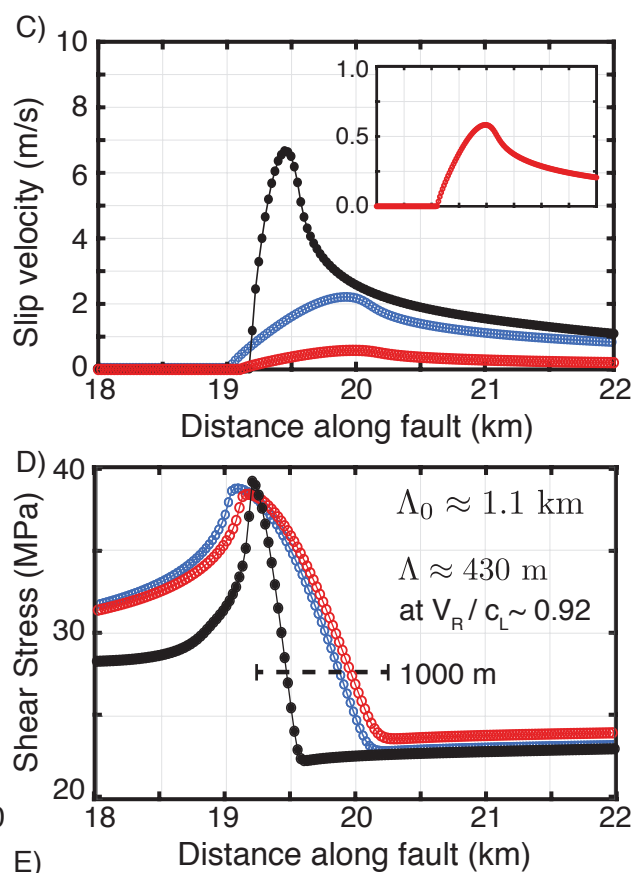
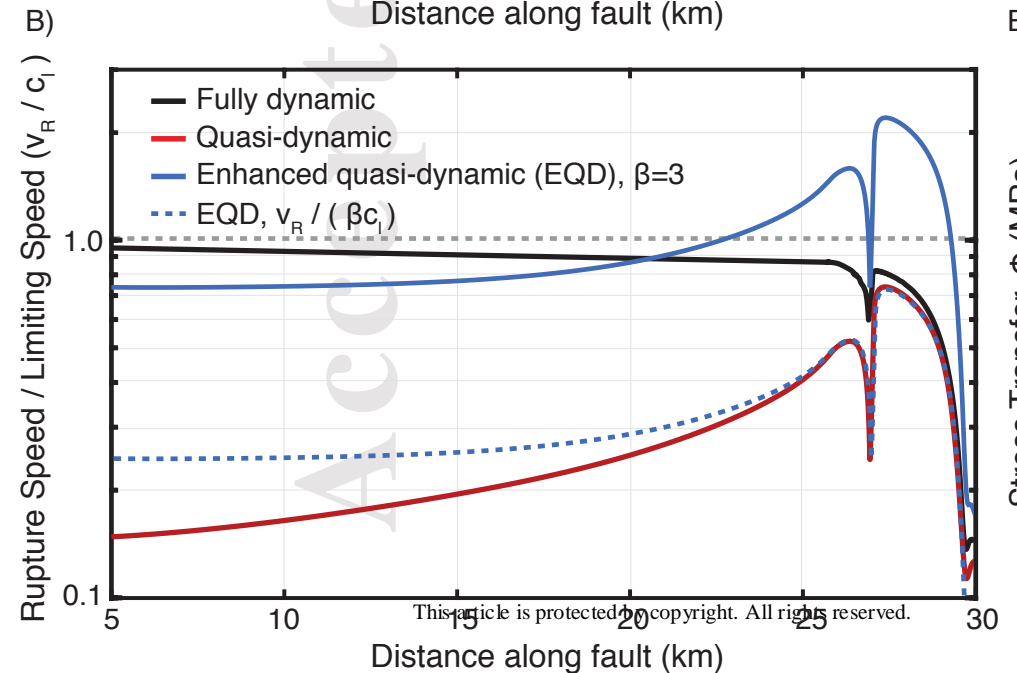
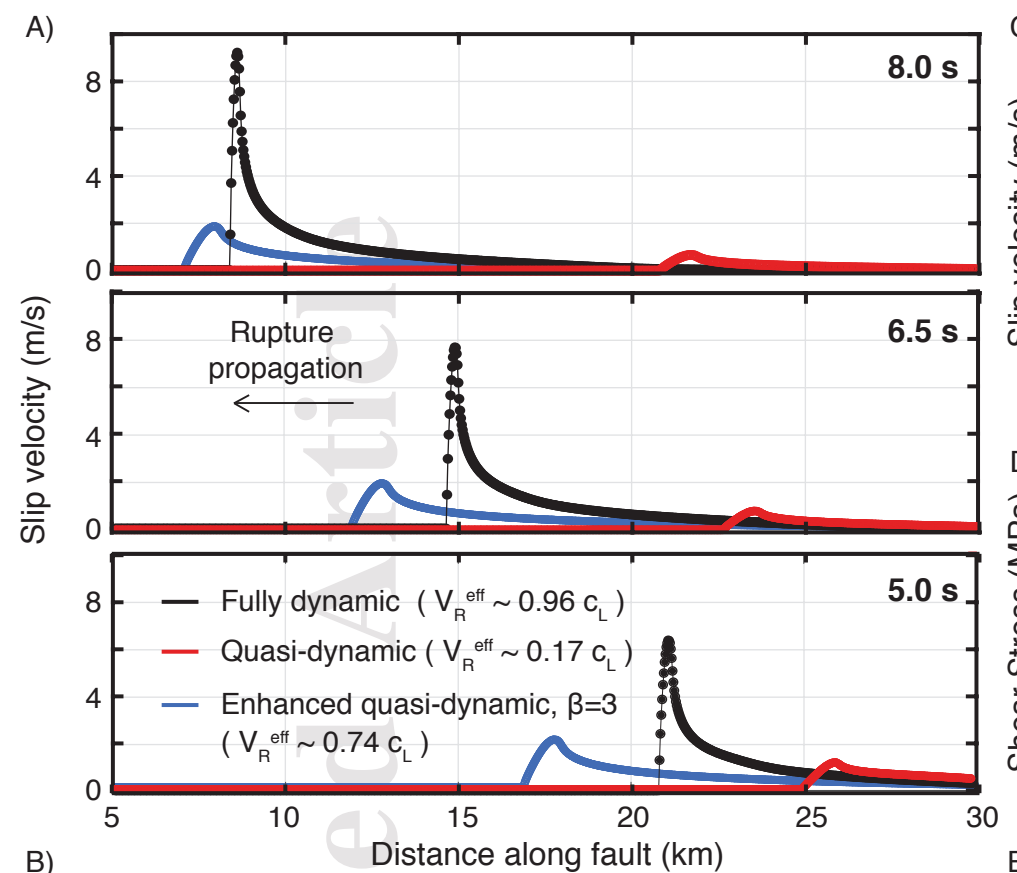


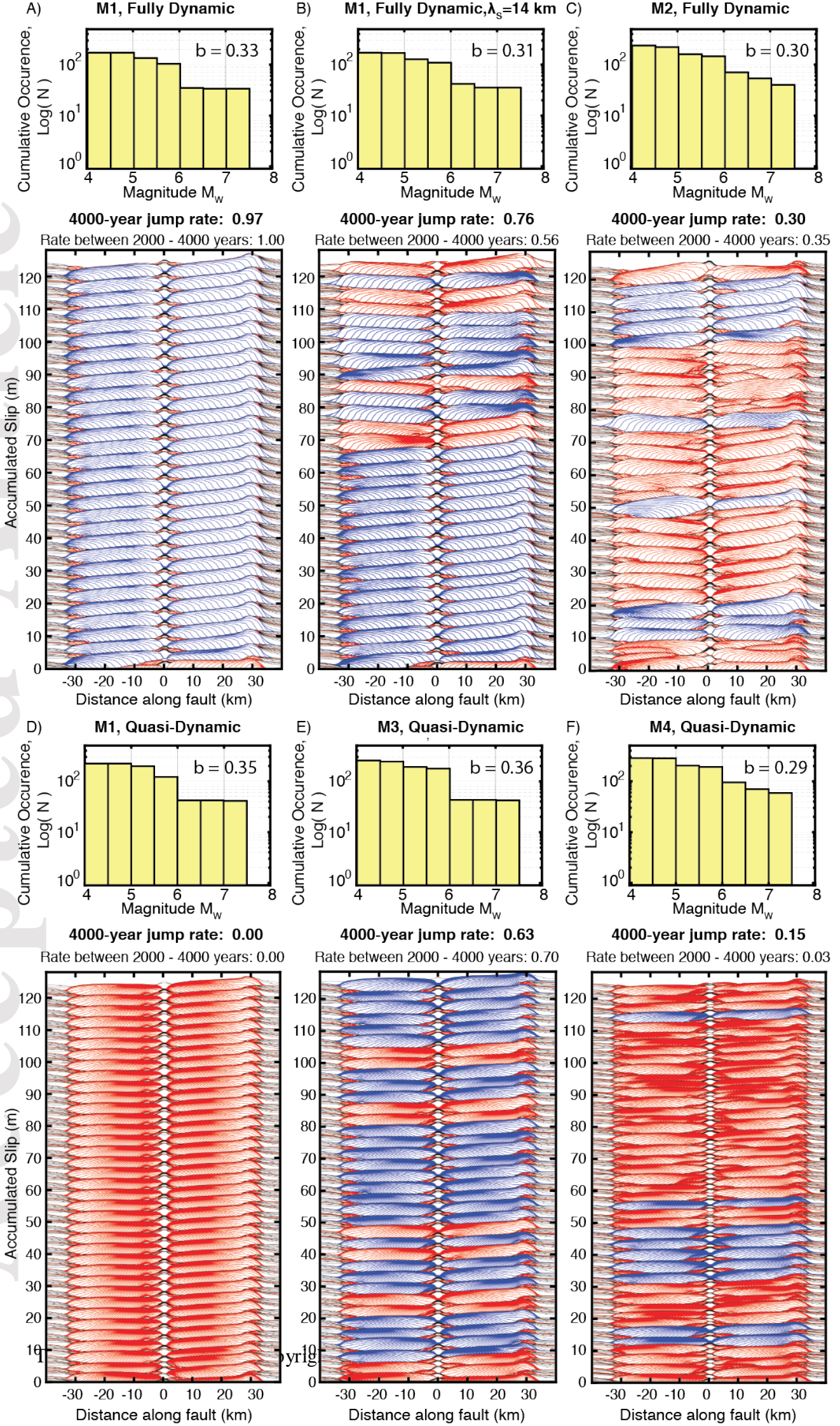
### Initial shear stress conditions S2

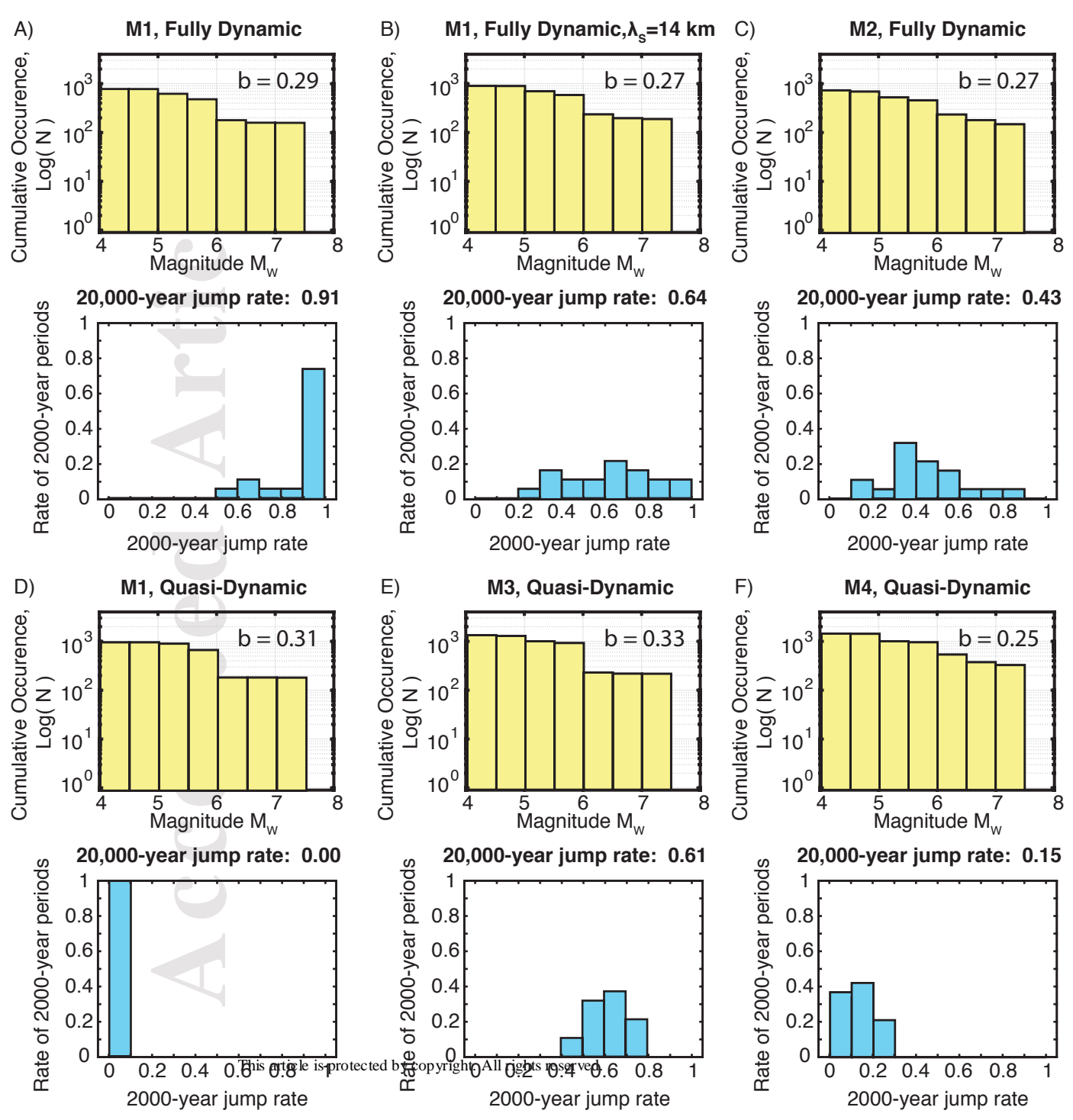


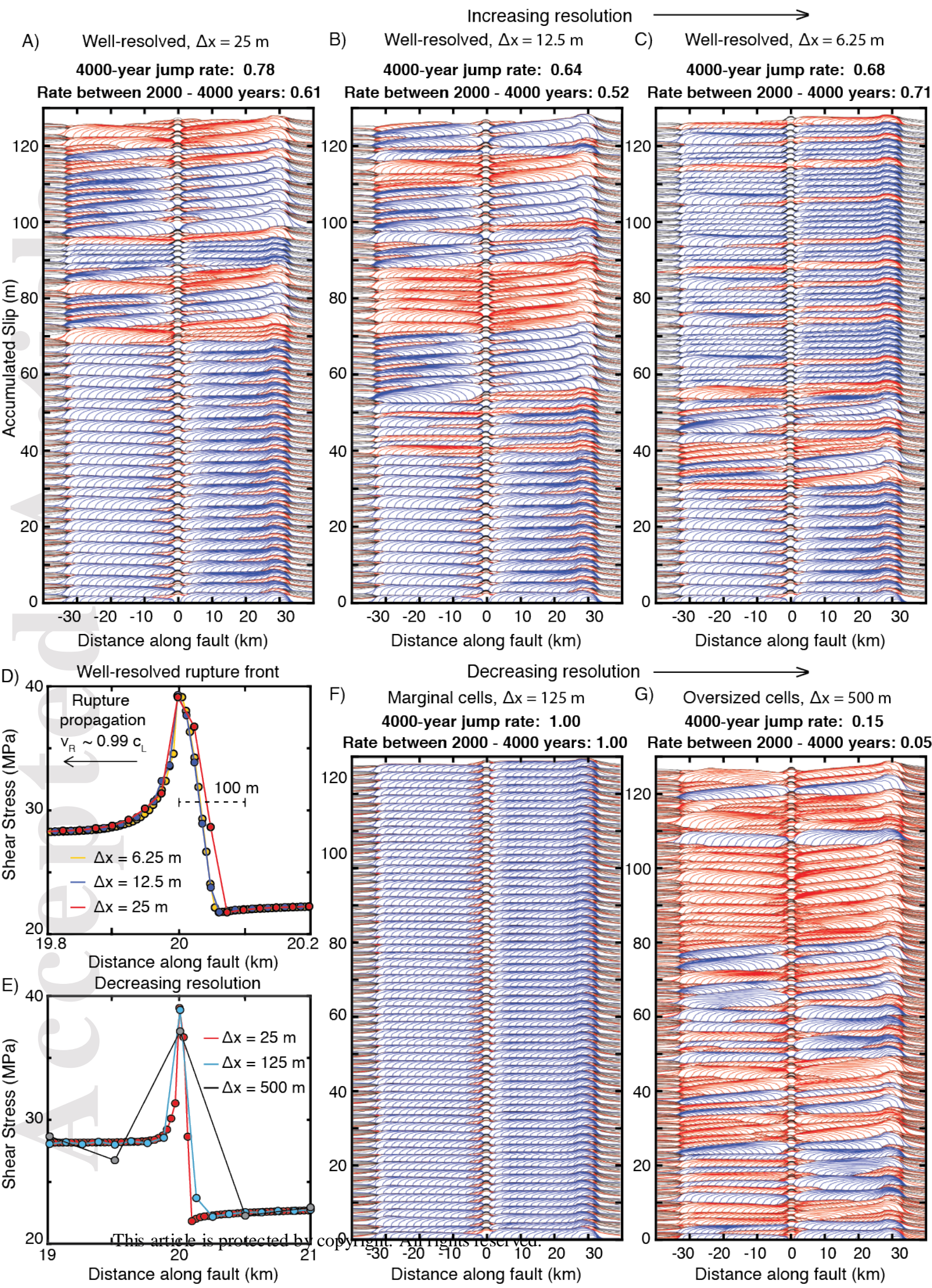
Article protected by copyright. All rights reserved.

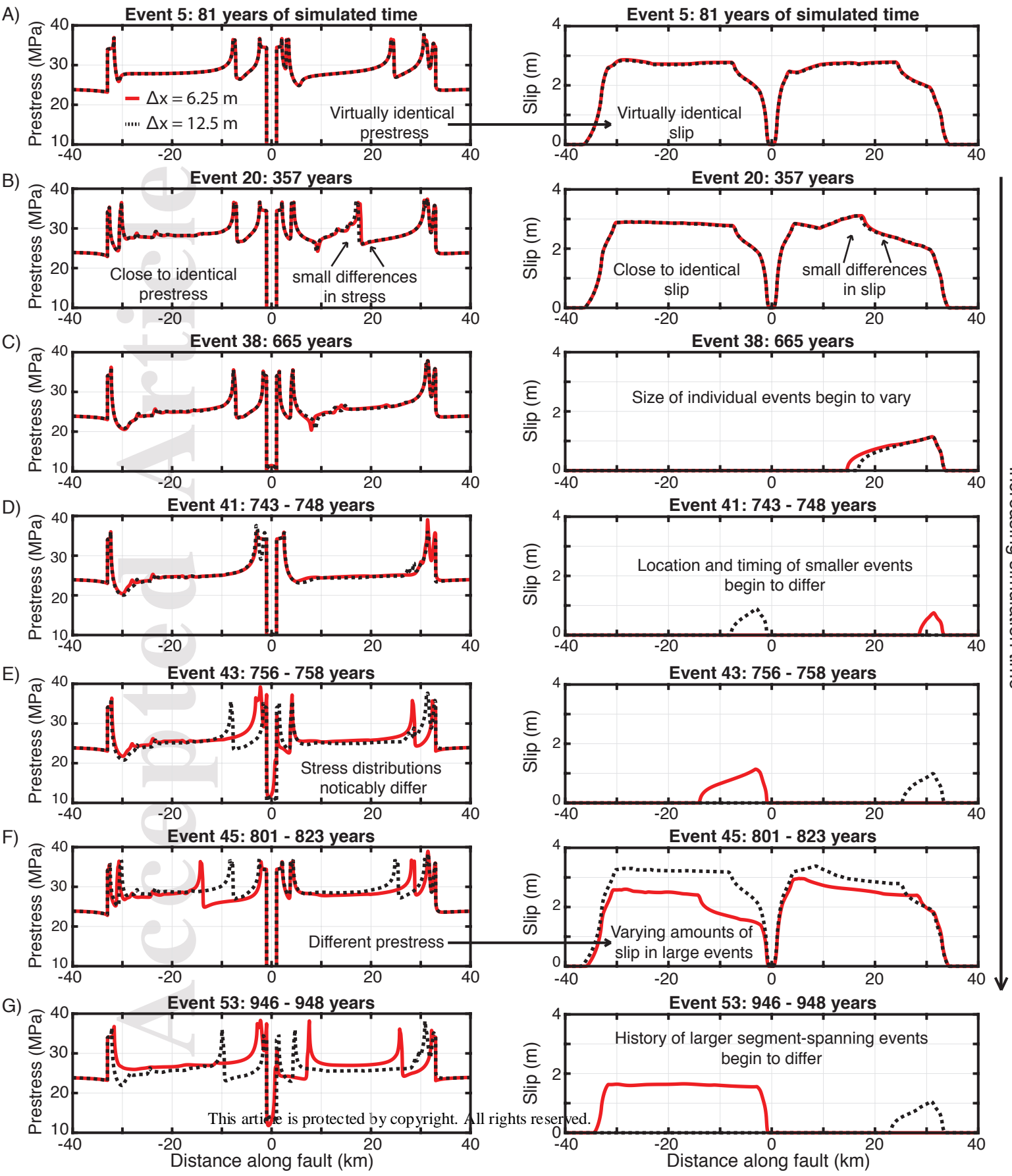


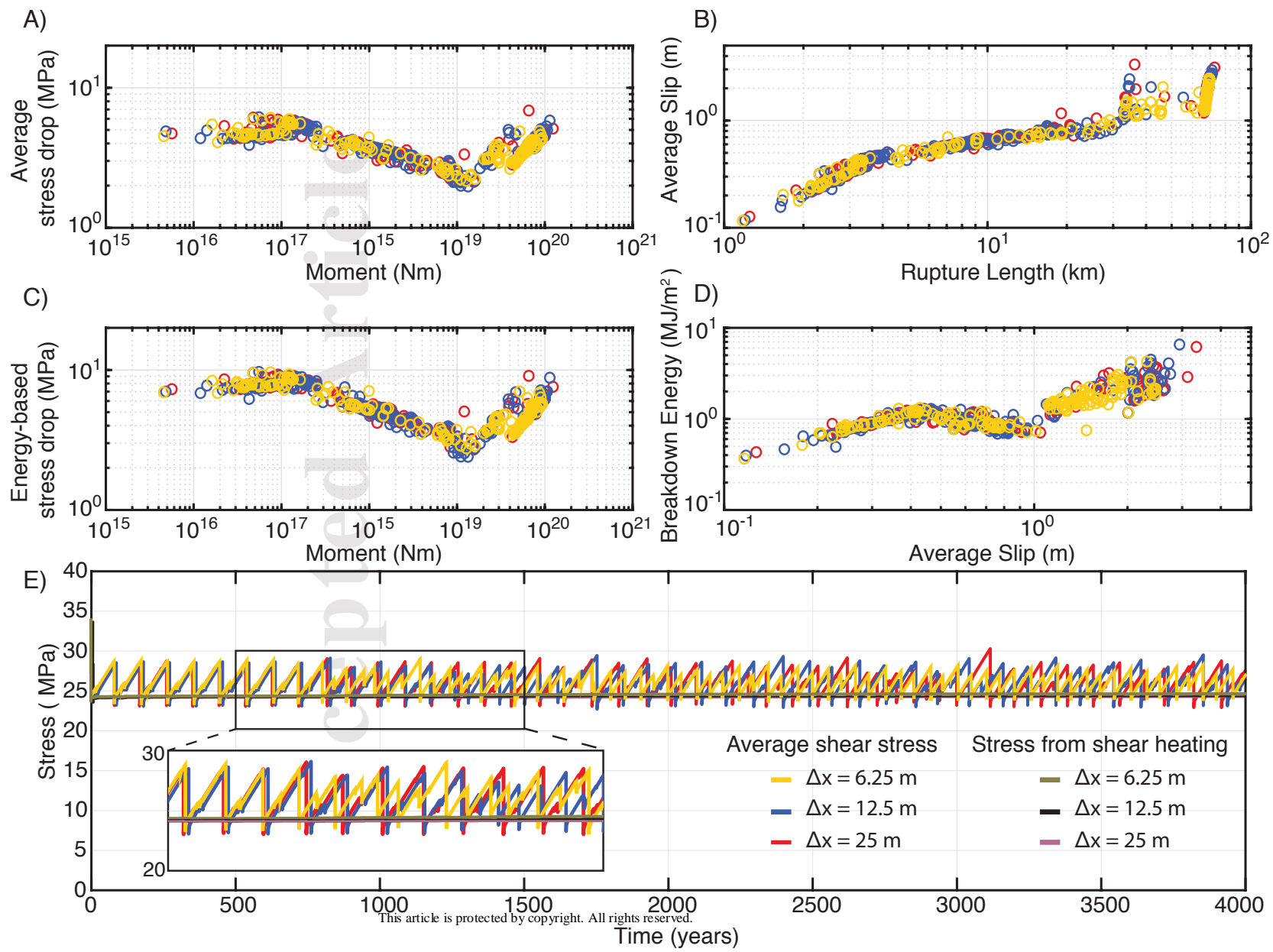


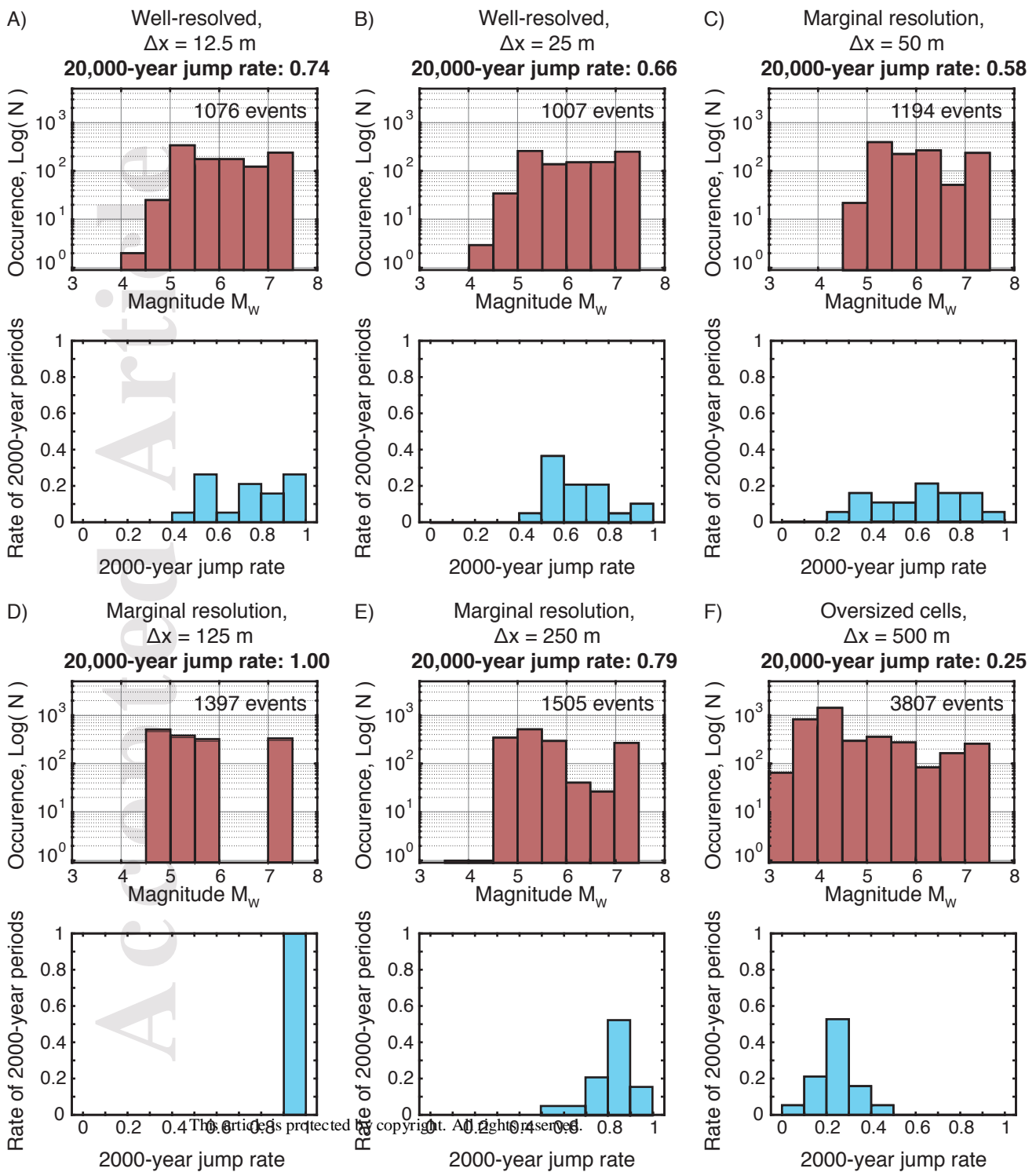


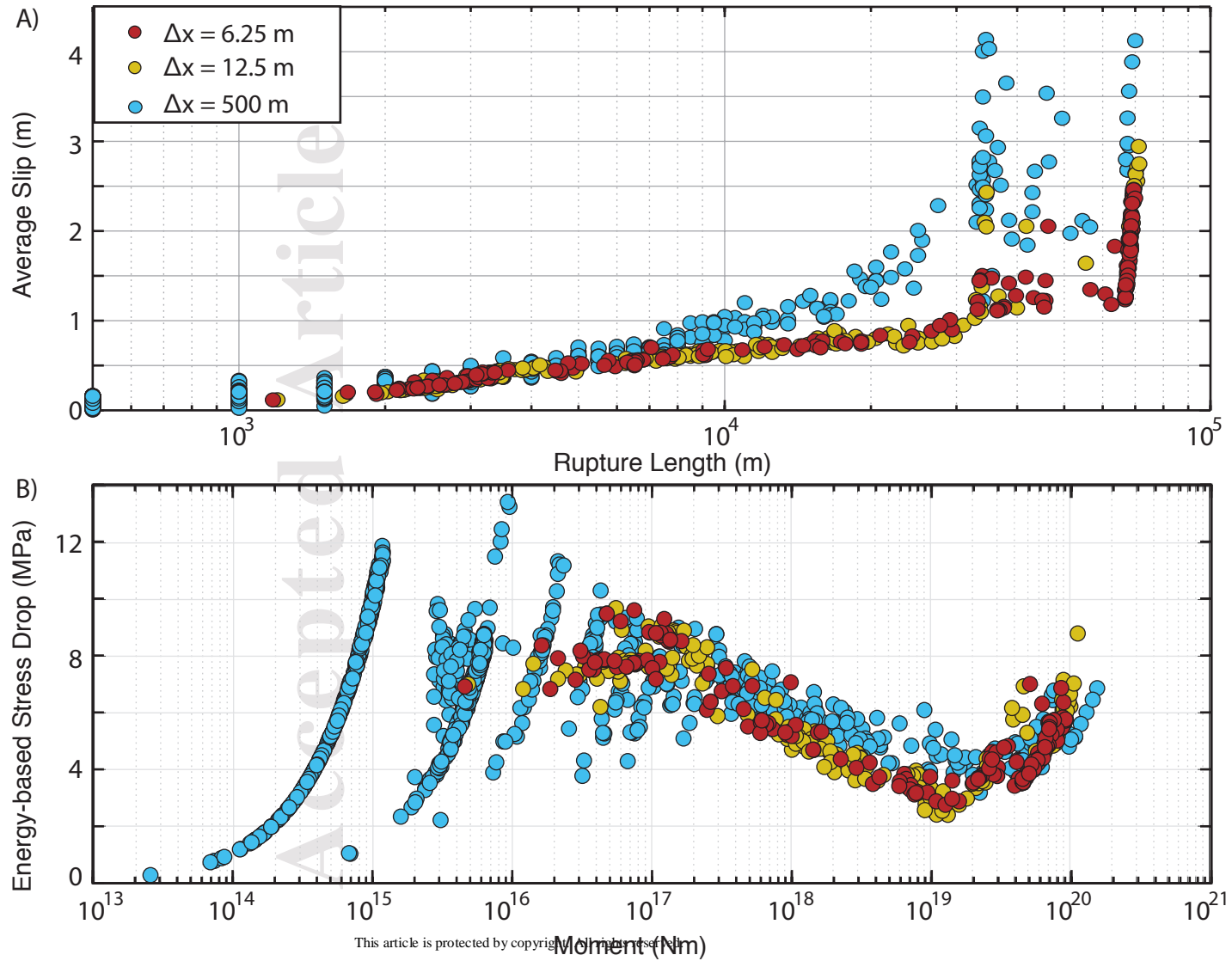


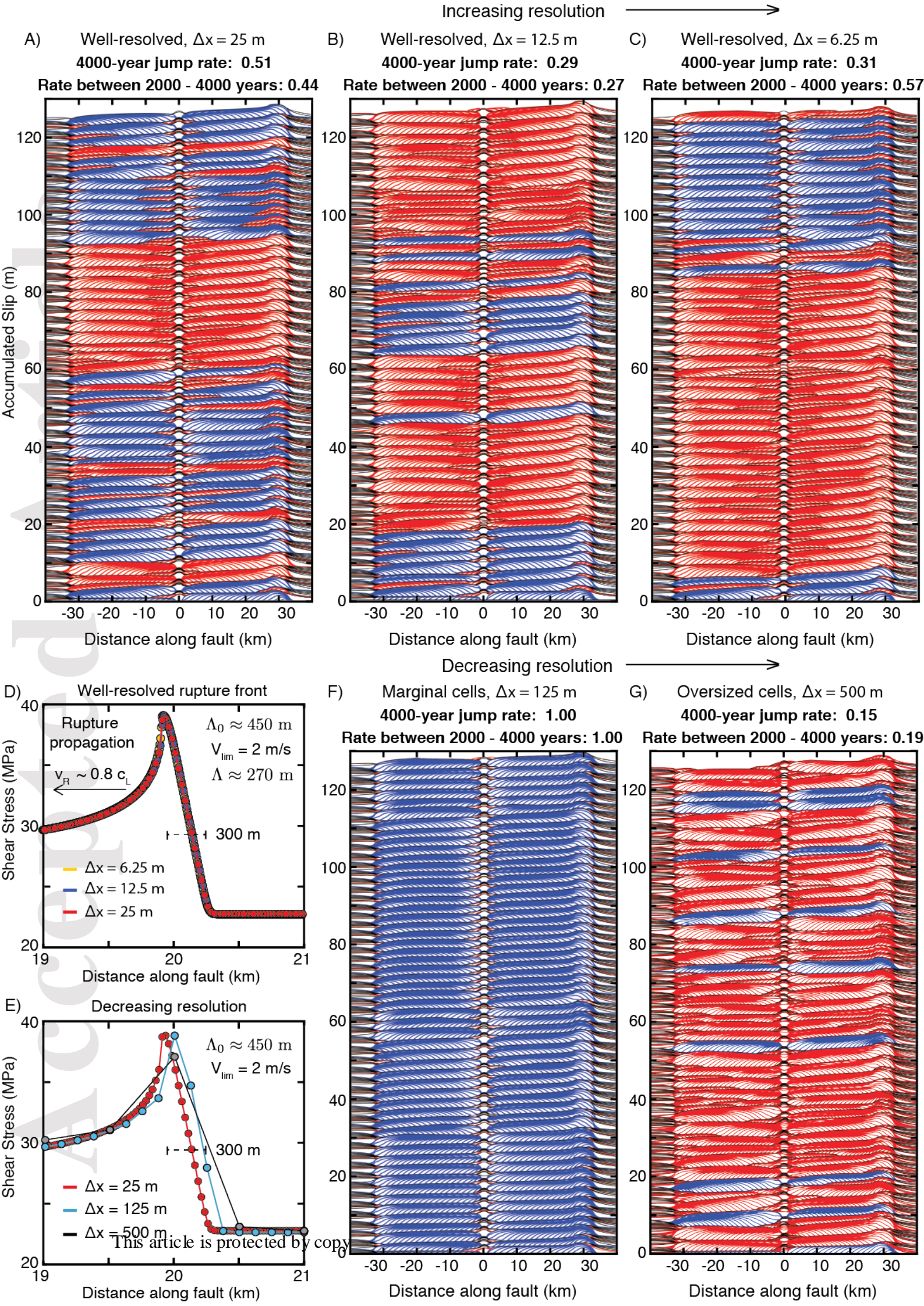




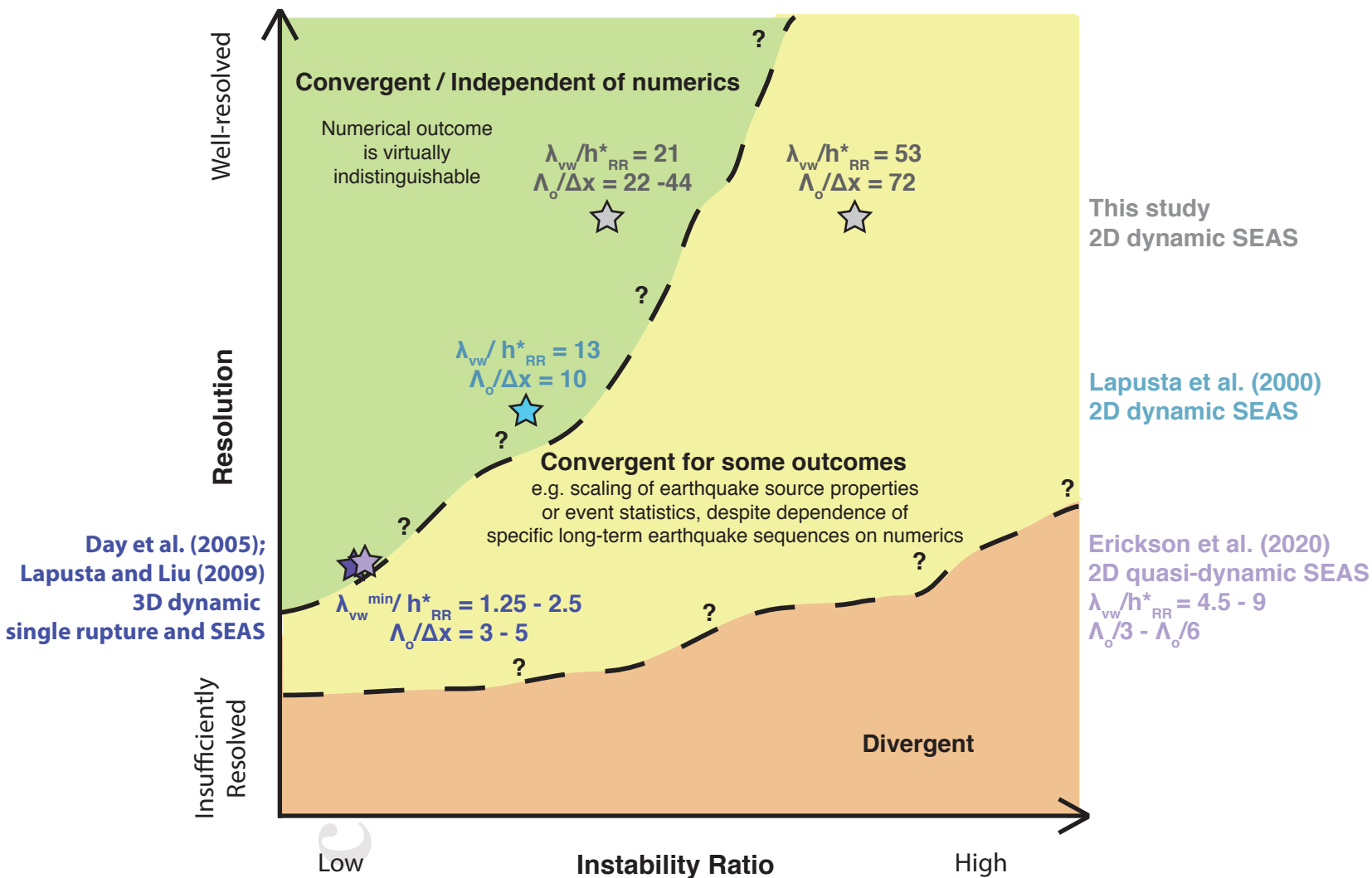








# Consistency among simulations of sequences of earthquakes and aseismic slip (SEAS)



- **Simulated outcomes converge and can be reliably determined upon sufficient discretization**
- **Some simulated outcomes may be reliably determined upon sufficient discretization, however others may considerably vary depending on numerical procedures**
- **Simulated outcomes exhibits clear dependence on numerical procedures**

This article is protected by copyright. All rights reserved.

Larger VS barrier,  $\lambda_B = 10$  km

